Multiomics Analyses Reveal Dynamic Bioenergetic Pathways and Functional Remodeling of the Heart During Intermittent Fasting

Thiruma V. Arumugam[1,2,3,#,*], Asfa Alli-Shaik[4,#], Elisa A. Liehn[5,6,7], Sharmelee Selvaraji[2,8], Luting Poh[2], Vismitha Rajeev[2], Yoonsuk Cho[3], Yongeun Cho[3], Jongho Kim[3], Joonki Kim[2,9], Hannah L. F. Swa[4], David Tan Zhi Hao[2], Chutima Ratttanasopa[10,11], David Yang-Wei Fann[2], David Castano Mayan[10], Gavin Yong-Quan Ng[2], Sang-Ha Baik[2], Karthik Mallilankaraman[2], Mathias Gelderblom[12], Grant R. Drummond[1], Christopher G. Sobey[1], Brian K. Kennedy[2,13], Roshni R. Singaraja[10,14], Mark P. Mattson[15], Dong-Gyu Jo[3], Jayantha Gunaratne[4,16,*]

[1]Centre for Cardiovascular Biology and Disease Research, Department of Microbiology, Anatomy, Physiology and Pharmacology, School of Agriculture, Biomedicine and Environment, La Trobe University, Bundoora, Victoria, Australia
[2]Department of Physiology, Yong Loo Lin School Medicine, National University of Singapore, Singapore
[3]School of Pharmacy, Sungkyunkwan University, Suwon, Republic of Korea
[4]Translational Biomedical Proteomics Laboratory, Institute of Molecular and Cell Biology, Agency for Science, Technology and Research, Singapore
[5]National Heart Research Institute, National Heart Centre Singapore
[6]Institute for Molecular Medicine, University of Southern Denmark, Odense, Denmark
[7]National Institute of Pathology "Victor Babes", Bucharest, Romania
[8]NUS Graduate School for Integrative Sciences and Engineering, National University of Singapore, Singapore
[9]Natural Products Research Center, Korea Institute of Science and Technology, Gangneung, Gangwon-do, Republic of Korea
[10]Translational Laboratories in Genetic Medicine, Agency for Science, Technology and Research, Singapore
[11]Cardiovascular and Metabolic Disorders Program, Duke-National University of Singapore
[12]Department of Neurology, University Medical Center Hamburg-Eppendorf, Germany
[13]Department of Biochemistry, Yong Loo Lin School Medicine, National University of Singapore, Singapore
[14]Department of Medicine, Yong Loo Lin School of Medicine, National University of Singapore, Singapore
[15]Department of Neuroscience, Johns Hopkins University School of Medicine, Baltimore, MD, USA
[16]Department of Anatomy, Yong Loo Lin School of Medicine, National University of Singapore, Singapore

Correspondence: Jayantha Gunaratne, Institute of Molecular and Cell Biology, Agency for Science, Technology and Research (A*STAR), Singapore, Singapore. E-mail: jayanthag@imcb.a-star.edu.sg or Thiruma V. Arumugam, Centre for Cardiovascular Biology and Disease Research, Department of Microbiology, Anatomy, Physiology and Pharmacology, School of Agriculture, Biomedicine and Environment, La Trobe University, Bundoora, Victoria, Australia. E-mail: g.arumugam@latrobe.edu.au

[#]These authors contributed equally to this work

Key words
Intermittent fasting, heart, mouse, RNA sequencing, proteomics, phosphoproteomics, metabolism, echocardiogram

Abstract

Aims

Intermittent fasting (IF) reduces cardiovascular risk factors in animals and humans, and can protect the heart against ischemic injury in models of myocardial infarction, but the underlying molecular mechanisms are unknown. To delineate molecular and cellular adaptations of the heart to IF, we carried out system-wide comprehensive analyses of proteome and phosphoproteome, complemented with transcriptome profiling, followed by functional analysis.

Methods and results

In order to understand molecular and cellular remodeling of the heart during IF, we employed advanced mass spectrometry for system-wide profiling of the proteome and phosphoproteome of heart tissues obtained from mice maintained for 6 months on either daily 12- or 16-hour fasting, every-other-day fasting or ad libitum control feeding regimens. We also performed transcriptome analyses using RNA sequencing to evaluate whether the observed molecular responses to IF occur at the transcriptional or post-transcriptional levels. IF regimens significantly affected pathways that regulate cyclic GMP signaling, lipid and amino acid metabolism, cell adhesion, cell death, and inflammation. Comparison of differentially expressed proteome and transcriptome upon IF showed the higher correlation of pathway alternation in short IF regimen but the inverse correlation of metabolic processes such as fatty acid oxidation and immune processes in longer IF regimens. In addition, functional echocardiographic analyses demonstrated that IF enhances stress-induced cardiac performance.

Conclusion

Our systematic multi-omics study elucidates a molecular framework for understanding how IF impacts the heart's function and its vulnerability to injury and disease.

Translational perspective

Intermittent fasting is emerging as a desirable lifestyle adaptation to impact cardiovascular health through the modulation of molecular and cellular mechanisms, and by acting on disease risk factors. Evidence from numerous studies indicates that the fasting cycles are highly and consistently effective in protecting against cardiovascular diseases and improving cardiac health in animals and human. Using multi-omics, here we dissect distinct molecular adaptations of the heart to different intermittent fasting regimens. Our results unveil novel cardioprotective mechanisms and open up new avenues for innovative pharmacological approaches to prevent and treat cardiovascular diseases.

1. Introduction

In the developed world, the average calorie intake has steadily risen, as have associated age-related diseases[1]. Intermittent fasting (IF) eating patterns include frequent periods of 12 to 24 hours with little or no energy intake sufficient to trigger a metabolic switch from the utilization of liver-derived glucose to fatty acids and ketones. Such IF eating patterns increase health span and lifespan and delay or prevent age-associated diseases in animals[2,3]. Rodents maintained on IF exhibit reduced resting heart rate and blood pressure, increased heart rate variability, and improved cardiovascular adaptations to stress[4-7]. Age-related increases in oxidative stress, inflammation, and fibrosis in the heart are prevented by every-other-day (EOD) fasting[8]. IF also improves health indicators and cardiovascular risk factors in human subjects[9-12]. In a recent randomized controlled trial, alternate day fasting improved cardiovascular markers, reduced fat mass, fat-to-lean ratio, and increased levels of the ketone β-hydroxybutyrate (BHB)[13]. IF protects the brain and heart against ischemic injury and enhances endurance in animal models[14-18]. Animals maintained on EOD fasting prior to experimental myocardial infarction (MI) have a reduced myocardial infarct size compared to the ad libitum (AL) fed controls[19-21]. IF also improves survival and recovery of heart function when initiated two weeks after MI[22]. Recent brain and skeletal muscle studies suggest that IF engages signaling pathways that enhance cellular stress resistance, mitochondrial biogenesis, and autophagy[16,17]. The ketone BHB may mediate some cellular adaptations to fasting, including inducing the expression of the inhibitory neurotransmitter γ-aminobutyric acid, trophic factors, and the cytoprotective mitochondrial deacetylase sirtuin 3[23-27]. However, it is unknown whether similar molecular and cellular mechanisms underlie the beneficial effects of IF on the cardiovascular system.

System-wide interrogation using large-scale omics technologies has proven powerful in capturing snapshots of molecular abundances in an unbiased manner. Previous studies have extensively focused on understanding the metabolic rewiring associated with different modes of fasting and feeding responses in the liver, the primary metabolic and secretory organ, and adipose tissues that functions as a fat sensor[28]. Though transcriptomics remained the go-to technology for many of the earlier works in this arena, recent technological advancements have positioned mass spectrometry (MS)-based proteomics as a rational choice to simultaneously track the dynamic behavior of thousands of proteins, the prime orchestrators of cellular processes, in a global manner. Accordingly, proteotypes underlying various metabolic diseases, dietary milieu, and fasting regimens including time-restricted feeding or IF have been probed to get holistic molecular portraits of altered metabolic states[29,30]. Protein post-translational modifications, especially phosphorylation, underlie several energy sensor pathways, glucose homeostasis mechanisms, and insulin secretion process, and hence deconvolution of phosphorylation networks is key to understanding signaling alterations[31,32]. While the importance of IF in improving cardiovascular health has been extensively documented, a global investigation documenting the molecular players that drive the metabolic switch would be highly desirable.

In order to understand molecular and cellular remodeling of the heart during IF, we employed advanced mass spectrometry for system-wide profiling of the proteome and phosphoproteome of heart tissues obtained from mice with daily fasting for 12 hours (IF12), 16 hours (IF16) or EOD as well as AL control feeding. We also performed transcriptome analyses using RNA sequencing to evaluate whether the observed molecular responses to IF occur at the transcriptional or post-transcriptional levels. Our results indicated that IF profoundly modifies pathways involved in metabolism, cell signaling, and epigenetic reprogramming in the heart. Of note, we observed that protein network remodeling during IF occurred in an IF duration time-dependent manner, with IF16 and EOD having the most significant effects. In addition, functional studies indicated that IF improves cardiac function compared to AL feeding. Our findings provide novel insight into the genetic and proteomic changes by which IF improves cardiac health and provide a resource for investigators in the fields of metabolism and cardiovascular disease.

2. Materials and methods

2.1 Animals and IF procedures

All *in vivo* experimental procedures were approved by the National University of Singapore and La Trobe University Animal Care and Use Committees and performed according to the guidelines set forth by the National Advisory Committee for Laboratory Animal Research (NACLAR), Singapore, and Australian Code for the Care and Use of Animals for Scientific Purposes (8th edition) and confirmed NIH Guide for the Care and Use of Laboratory Animals. All efforts were made to minimize suffering and the number of animals used. All sections of the manuscript were performed in accordance with ARRIVE guidelines. Animals were anaesthetized in 1-2 % isoflurane, and anesthesia was confirmed by abolished pain reflexes. Animals were euthanized by cervical dislocation, and the chest was then opened to extract the heart. C57BL/6 male mice were purchased at 2 months of age (InVivos, Singapore; ARC, Australia) and housed in the animal facility at the National University of Singapore and La Trobe University. The animals were exposed to light from 07:00-19:00 (12 hours light: 12 hours dark cycle) and were fed with pellets for rodents which consisted of 58%, 24%, and 18% of calories originating from carbohydrate, protein, and fat, respectively (Teklad Global 18% Protein rodent diet #2918; Envigo, Madison, WI, USA). Water was provided ad libitum to all dietary groups. At the age of 3 months, the mice were randomly assigned to the four different dietary intervention groups: IF12 (N=20), IF16 (N=60), EOD (Every Other Day fasting) (N=20), and AL group as a control (N=60). The mice in the IF12, IF16, and EOD groups fasted for 6 months daily 12 hours (19:00-07:00), 16 hours (15:00-07:00), or 24 hours (a whole day fasting followed by an entire day feeding). The AL group was supplied with food pellets ad libitum. The body weight was regularly measured. Blood glucose and ketone levels using FreeStyle Optium Neo system with FreeStyle Optium blood glucose and ketone test strips (Abbott Laboratories, Berkshire, UK) were measured in the morning before IF animals received food (N=20 in each experimental group). After 6 months, animals were anesthetized and euthanized. EOD mice were euthanized on a food-deprivation day. All mice were euthanized under isoflurane anesthesia between 7 a.m. and noon. All mice were perfused with cold PBS. The chest cavity was rapidly opened, and the heart was removed and rinsed in two washes of ice-cold saline. Major blood vessels and connective tissue were removed, and the heart was blotted dry, and weighed. The heart samples were collected and kept at -80°C until further use.

2.2 Sample preparation for proteome analyses

Frozen tissue samples from all groups (Number of animals in AL=4, IF12=5, IF16=5, EOD=4) were crushed in liquid nitrogen prior to lysis with 6M urea (Sigma-Aldrich), 2 M thiourea (Invitrogen), and 20mM HEPES. The lysate was collected after centrifugation at 20,000g for 20min at 15°C, and protein measurement was made using Pierce™ 660nm Protein Assay Reagent (Thermo Scientific™) according to the manufacturer's protocol. 50 μg of protein was used to prepare for each TMT label. For the reference channel of 126-TMT label, a total of 50 μg protein pooled from the 4 ALs was used. The reduction was performed with a final concentration 5 mM dithiothreitol (Sigma-Aldrich) incubation for 30min. This was followed by alkylation with a final concentration of 10mM iodoacetamide (Sigma-Aldrich) for 30min incubation in the dark. Digestion was carried out using lysyl endopeptidase digestion (Wako Chemicals GmbH) with enzyme: protein = 1:100 at 37°C overnight. The urea in the lysis buffer was then diluted to a final concentration of 1 M with 50 mM ammonium bicarbonate followed by trypsin digestion (Promega) with enzyme: protein = 1:50 at 37°C for 8 hours. Digested peptides were desalted using 1ml Empore C18 cartridges (3M) before isobaric labeling.

2.3 Sample preparation for phosphoproteome analysis

A total of 3 animals from each group were used for phosphoproteome analysis. Immobilized metal affinity chromatography (IMAC) was employed for the selective enrichment of phosphorylated peptides. Briefly, Ni-NTA agarose conjugates (Qiagen) were rinsed thrice with MilliQ water and incubated with 100mM EDTA pH 8.0 for 30 min at RT to strip the nickel. Residual nickel was rinsed thrice with MilliQ water, followed by incubation with 100 mM iron chloride solution for 30-45 min. The resin was then washed thrice with MilliQ water followed by 80% acetonitrile / 0.1% trifluoroacetic acid. The tryptic peptides were then enriched using the iron chloride treated IMAC beads. Tryptic peptides were reconstituted in 50% acetonitrile/0.1% trifluoroacetic acid, followed by 1:1 dilution with 99.9% acetonitrile/0.1% trifluoroacetic acid. The peptides were incubated with 10 μL of IMAC beads for 30 min with end-over-end rotation, and the beads were subsequently loaded onto self-packed C18 stage tips[33] pretreated with 200 μl methanol, washed with 50% acetonitrile/0.1% formic acid and equilibrated with 1% formic acid. Following loading onto the stage tip, the IMAC beads were washed with 80% acetonitrile/0.1% trifluoroacetic acid and 1% formic acid. The phosphopeptides were eluted from the IMAC beads onto C18 membranes using 500 mM dibasic sodium phosphate (pH 7.0), followed by washing using

1% formic acid. The phosphopeptides were stored on the stage tip until they were ready to be analysed by LC-MS. The phosphopeptides were eluted from the C18 membranes with 50% acetonitrile/0.1% formic acid, dried using a speed vac, and reconstituted in 0.1% formic acid for LC-MS analysis.

2.4 Isobaric labeling

All samples were run in a total of two sets of TMT10plex™ Isobaric Label Reagent Set (Thermo Scientific™) and were assigned to each TMT set (9 samples to 9 plexes and an internal reference sample made up of a mixture of the ALs) by randomization. Isobaric labelling was performed according to the manufacturer's protocol. Briefly, the TMT label was reconstituted in anhydrous acetonitrile (Sigma-Aldrich) before mixing with respective peptides and incubated for 1 h. The reaction was quenched using the final 5% hydroxylamine (Merck) in triethylammonium hydrogen carbonate buffer (Fluka) for 15 min. Labeled peptides were mixed before being vacuum-dried and fractionated using basic reverse phase chromatography (Shimadzu NexeraXR high performance liquid chromatography). Fractions were combined orthogonally into 15 fractions and dried using a vacuum centrifuge.

2.5 Liquid chromatography and mass spectrometry

For proteome analysis, peptides were reconstituted in 0.1% formic acid for analysis on Thermo Easy nLC 1000 that was connected to Q Exactive™ Plus Hybrid Quadrupole-Orbitrap™ Mass Spectrometer (Thermo Scientific™). The trap column used was C18 Acclaim PepMap™ 100 of 5 μ m, 100A, 100 μ m I.D. x 2 cm, and the analytical column was PepMap™ RSLC C18, 2 μ m, 100A, 75 μ m I.D. x 50 cm. The LC solvent A comprised of 0.1 M formic acid in 2% acetonitrile, and LC solvent B comprised 0.1 M formic acid in 95% acetonitrile. The gradient was as follows: 5–50% solvent B in 180 min; 50-100% solvent B in 10 min; 100% solvent B for 10 min at the flow rate of 200 nL/min. The mass spectrometer was set in the data dependent acquisition mode. Full scan MS spectra (m/z 380 – 1600) were acquired with a resolution of R=140,000 at an AGC target of 3e6 and a maximum injection time of 60 ms. The top 20 most intense peptide ions in each MS scan were sequentially isolated to an ACG target value of 1e5 with a resolution of 35,000 and fragmented using a normalized collision energy of 30 at MS2 level with fixed first mass at 110 and an isolation

window of 1.2 m/z. For phosphoproteome, reconstituted peptides were analysed using an EASY-nLC 1000 (Proxeon, Fisher Scientific) attached to a Q-Exactive (Thermo Fisher Scientific). Peptides were enriched using a C18 precolumn and separated on a 50 cm analytical column (EASY-Spray Columns, Thermo Fisher Scientific) at 50°C using a 265 min gradient ranging from 0 to 40% acetonitrile/0.1% formic acid, followed by a 10 min gradient ranging from 40 to 80% acetonitrile/0.1% formic acid and maintained for 10 min at 80% acetonitrile/0.1% formic acid. Survey full scan MS spectra (m/z 310–2000) were collected with a resolution of r = 70,000, an AGC target of 3e6, and a maximum injection time of 10 ms. Twenty of the most intense peptide ions in each survey scan with an intensity threshold of 10,000, underfill ratio of 1%, and a charge state ≥ 2 were sequentially isolated with a window of 2 Th to a target value of 50,000 with a maximum injection time of 50 ms. These were fragmented in the high energy collision cell by dissociation, using a normalized collision energy of 25%. The MS/MS was acquired with a starting mass of m/z 100 and a resolution of 17,500 and dynamic exclusion of duration of 15 s.

2.6 Total RNA extraction and quality control for transcriptome analyses

EZ-10 Total RNA Mini-Prep Isolation kit (Bio Basic, Canada) was used according to the kit's instructions to extract total RNA from the heart samples. To assess the quality of the extracted total RNA, agarose gel electrophoresis and Agilent Bioanalyzer 2100 system (Agilent, Santa Clara, CA, USA) were used. All RNA samples (N=5 in each experimental group) had high quality with integrity numbers > 6.9 for total RNA.

2.7 cDNA library preparation and RNA sequencing

Poly-T oligo-attached magnetic beads were used to purify the mRNA from total RNA. Then, a fragmentation buffer was added to the mRNA. First-strand cDNA was subsequently synthesized using random hexamer primer and M-MuLV reverse transcriptase (RNase H-) (New England BioLabs, Ipswich, MA, USA). Next, second-strand cRNA synthesis was performed using DNA polymerase I and RNase H. AMPure XP beads (Beckman Colter Life Sciences, Indianapolis, IN, USA) were used to purify the double-stranded cDNA. By using exonuclease/polymerase activities, the remaining overhangs of the purified double-stranded cDNA were transformed into blunt ends. The 3' ends of the DNA fragments were adenylated, followed by ligation of the NEBNext adaptor with a hairpin loop structure to prepare for hybridization. The library fragments were purified with the AMPure XP system to select cDNA with the base pair length of 150-200. Lastly, the library was amplified by polymerase

chain reaction (PCR), and the PCR products were purified using AMPure XP beads. The HiSeq™ 2500 platform (Illumina, San Diego, CA, USA) was used to conduct the high-throughput sequencing.

2.8 Transcriptome data mapping and differential expression analyses

The RNA sequencing results from the HiSeq system were output as quality and color space fasta files. The files were mapped to the Ensembl-released mouse genome sequence and annotation (Mus musculus; GRCm38/mm10). Bowtie v.2.0.6 Indexes were used to build the reference genome, and TopHat v.2.0.9 with a mismatch parameter limited to 2 was used to align the paired-end clean reads to the reference genome. 48.5 million clean reads were generated per sample, and 43.7 million reads (90.1% of total clean reads) per sample were mapped to the reference genome. HTSeq v.0.6.1 was used for the quantification of gene expression levels to count the read numbers mapped of each gene. Then FPKMs of each gene were calculated based on the length of the gene and reads count mapped to the same gene. DESeq R Package v.1.10.1 was used to perform differential expression analysis. To control the false discovery rate, the p-values resulting from the analysis were adjusted to q-values using Benjamini and Hochberg's approach. Genes with q-value < 0.05 found by DESeq were assigned as differentially expressed.

2.9 Heat map generation and functional enrichment analyses

R and the R package heatmap3 were used along with the log2 fold change output from EdgeR v.3.2.4 to create heatmaps of DEGs. To estimate the possible biologic functional changes derived from the gene expression changes, gene ontology (GO) and Kyoto Encyclopedia of Genes and Genomes (KEGG) pathway enrichment analyses were conducted. GO enrichment analysis was implemented by the GOseq R package, in which gene length bias was corrected. For KEGG pathway enrichment analysis, we used KEGG Orthology Based Annotation System (KOBAS) software to test the statistical enrichment. GO terms and KEGG pathways with a q-value less than 0.05 were considered significantly enriched by DEGs.

2.10 Proteome and phosphoproteome data processing

For 10plex-TMT labeled proteome analysis, raw MS data were processed using Proteome Discoverer 2.2 (Thermo Scientific™). Database search was performed using the integrated Sequest HT search engine against the Uniprot mouse FASTA database (release January 2018) for tryptic peptides with a maximum of two missed cleavage sites, MS and MS/MS mass

tolerance of 10 ppm and 0.02 Da, respectively. Searches included cysteine carbamidomethylation and TMT-modifications at peptide N-termini and lysine residues as fixed modifications and protein N-terminal acetylation and methionine oxidation as dynamic modifications. Peptide and protein identifications were performed at a false discovery rate (FDR) < 0.01. For phosphoproteome analysis, raw MS data were processed using MaxQuant version 1.6.0.1[34]. The Andromeda search engine was employed to search against the UniProt mouse FASTA database. For identification of proteins, peptides, and modifications, the FDR was set at 0.01, allowing a maximum of two missed cleavages as well as an initial mass tolerance of 4.5 ppm for precursor ions and 20 ppm for fragment ions. The search was performed with phosphorylation of sites serine, threonine, and tyrosine (STY), oxidation of methionine, and acetylation of protein N-term as variable modification, cysteine carbamidomethylation as fixed modification, and trypsin as cleaving enzyme. Label-free quantitation (LFQ) was performed using the MaxLFQ algorithm as implemented in MaxQuant with minimum ratio count set to 1 and match between run feature enabled to transfer peptide identifications across MS runs (match time window = 2, alignment time window = 20)[35]. A minimum Andromeda score of 40 was used for phosphopeptide identification.

2.11 Proteome and phosphoproteome data analyses

For TMT-based proteome analysis, the common internal reference, pooled AL sample, at the 126 TMT-reporter channel of each TMT set was used for normalization across the two sets. The pooled ad libitum was included as an internal reference for the TMT sets as our focus was on inferring proteome abundance changes and associated biological pathways across the different IF regimens in comparison with the control ad libitum group. Protein abundances across all the channels were first normalized for equal total protein intensities before obtaining log2 ratios of each protein against the normalized intensity of the respective reference channel. After combining the two TMT sets, only those proteins that were quantified in at least three biological replicates within each group were retained for subsequent analysis. For differential expression analysis of proteins regulated with IF, the replicates from the two TMT sets were grouped, and one-way analysis of variance (ANOVA) was performed with followed by Dunnett's post hoc tests at adjusted p-value < 0.01 to test for pairwise significance testing against AL control group. Protein annotations for gene ontology (GO) terms (biological process, cellular component, and molecular function) and KEGG pathways were obtained, and functional enrichment analysis was performed using Fisher's

exact test (FDR ≤ 0.05) for the modulated clusters. In addition, 1-D annotation enrichment analysis as implemented in Perseus was performed for testing the preference of protein expression values to be higher or lower in comparison to the global distribution for specific functional groups[36]. The FDR was controlled at a threshold of 0.05, and for each functional group, a score was assigned, with scores those higher than zero and close to 1 confirming to positive enrichment, and those lesser than zero and close to -1 representing negative enrichment[37]. To construct functional networks over the different IF regimens, gene-set enrichment analysis (GSEA) was performed on the proteome data using all curated mouse GO biological processes and pathways. Pairwise comparisons of the different groups were performed, and the statistical significance of the enrichment score was assessed by a permutation test. Based on the similarity between enriched gene sets (p-value < 0.01), the EnrichmentMap plugin, as implemented in Cytoscape, was used to visualize all overlapping gene set clusters[38]. All heat maps corresponding to functional categories were visualized using an internal log-transformed reference normalized abundance value for each protein[39]. Transcription factor enrichment analysis for significant proteins in each IF group was performed using the Chip Enrichment Analysis (ChEA) implemented in the Enrichr web tool[40,41].

For phosphoproteome analysis, the label-free intensities of all identified phosphopeptides were log-transformed, and only those phosphopeptides quantified in at least two biological replicates of each group were retained for all subsequent analyses. Using the Perseus software environment, missing values were imputed to represent intensities of low abundant proteins based on random numbers drawn from a normal distribution in each sample[36]. Phosphorylation sites differentially regulated between the groups were identified using one-way ANOVA followed by Dunnett's post hoc test at an adjusted p-value ≤ 0.05. Biological processes and KEGG pathways for differentially altered phosphoproteins were derived from DAVID bioinformatics resources[42]. For upstream kinase enrichment analysis, kinase substrate motifs were extracted from the human protein reference database (HPRD), and enrichment analysis was performed using Fisher's exact test for altered phosphosite clusters across the groups.

2.12 Comparison of proteome and transcriptome data

For the evaluation of the proteome against the transcriptome, only those transcripts with corresponding protein quantification were used. Correlation analysis was performed using

FPKM as a proxy for mRNA abundance and normalized protein abundance derived from TMT experiments for protein quantification. Data were log-transformed prior to visualization. For comparison of transcriptome and proteome changes across different IF groups, log-transformed fold changes relative to AL group were used as input to perform two dimensional (2-D) functional enrichment analyses as implemented in Perseus[36]. The respective annotation matrix of KEGG pathways and GO terms (biological process) of both the transcriptome and proteome were compared for significant bias to larger or smaller expression values in comparison to overall distribution. The FDR was controlled at a 0.05 threshold and position score was assigned to denote enrichment at higher ($0 < score < 1$) and lower ($-1 < score < 0$) abundances. A Scatter plot was constructed based on the positional scores, and functional categories were highlighted.

2.13 Protein-protein interaction network analyses

Functional connectivity between significantly altered proteins was explored using protein-protein interactions curated in the Pathway Commons database, which compiles pathway and interaction data from multiple resources[43]. In addition to direct physical interaction between proteins, associations that represent functional interactions such as those that regulate expression, control protein state change, and catalysis, or mediate complex formation were also considered. The IF-altered functional network encompassed interactions relevant to all metabolic, regulatory as well as signaling pathways. Duplicate interactions were removed to remove redundancy, and the network was populated with information on the regimen-specificity of altered proteins to obtain time-resolved functional networks. Cluster assessment was performed using Cluster ONE implemented in Cytoscape to identify densely connected regions within the network (p-value < 0.1)[44,45]. The functional biases of the identified clusters for ontology and pathways were derived from DAVID bioinformatics resources[42]. Finally, the topological parameters of the network were assessed for node centrality and degree distribution.

2.14 Perturbation association network analyses

A correlation matrix was obtained based on the quantitative proteome from all groups using Spearman's rank correlation. The correlation coefficients and p values were calculated for all pairs of proteins, and multiple testing was controlled using Benjamini-Hochberg correction. Proteins pairs with adjusted p-value ≤ 0.01 were filtered to retain only those highly confident protein-protein associations (absolute correlation coefficient ~ 0.82) pertaining to both

positive and negative correlations. Unweighted correlation networks were assembled using the high confident associations, and following the 'interactome mapping by high-throughput quantitative proteome analysis' (IMAHP) method[46], specific deviations of each sample from the correlations were evaluated using Mahalanobis distance followed by outlier analysis using Grubbs's test (p-value $\leq$ 0.1) to identify perturbed associations in each sample. To identify consensus-perturbed proteins among different dietary groups, a hypergeometric test was performed against the background of all perturbations (p-value $\leq$ 0.05). Functional assessment of perturbed proteins in each group for processes and pathways were derived from DAVID bioinformatics resources[42]. For the construction of mitochondrial perturbation network, we extracted those perturbed proteins annotated "mitochondria" across all groups, along with their regimen-specific co-regulated associations to be visualized as a network with functional annotations.

2.15 Immunoblot analysis

Frozen heart tissue samples (N=6 in each experimental group) were homogenized using a tissue tearor (BioSpec, Model: 985370) with protein and phosphatase inhibitors and Tissue Protein Extraction Reagent (Thermo Scientific, 78510) as the lysis buffer. The heart tissue samples were then combined with 2 x Laemelli buffer (Bio-Rad Laboratories, Inc., Hercules, CA, USA). Protein samples were then separated on 7.5 to 20% v/v sodium dodecyl sulfate (SDS) gels. The SDS-PAGE gels were transferred onto nitrocellulose membranes to probe for proteins. Next, the nitrocellulose membranes were incubated with the following primary antibodies: p-AMPKα (2535S, Cell Signaling), AMPKα (2532, Cell Signaling), PKG-1 (3248S, Cell Signaling), MYPT1 (2634S, Cell Signaling), PPARγ (7273, Santa Cruz Biotechnology), p-GSK3α/β (9331S, Cell Signaling), GSK3α/β (7291, Santa Cruz Biotechnology), AKT (9272S, Cell Signaling), Insulin receptor β (3025S, Cell Signaling), Phospho-IRS1 (Ser318) (5610, Cell Signaling), IRS-1 (2382S, Cell Signaling), and GAPDH (2118S, Cell Signaling; NB300-221, Novus Biologicals) overnight at 4°C with agitation. After primary antibody incubation, membranes were washed three times with 1xTBST before incubating with horseradish peroxidase (HRP)-conjugated secondary antibodies (Goat Anti-Rabbit – Cell Signalling Technology, Danvers, MA, USA; Goat Anti-Mouse – Sigma-Aldrich, St. Louis, MO, USA) for 1 hour at 24°C with agitation. The membranes were then washed three times (10 min each) with 1xTBST. The substrate for HRP, enhanced chemiluminescence (ECL) (Bio-Rad Laboratories, Inc., Hercules, CA, USA), was applied for

3 min before the membranes were imaged using the ChemiDocXRS+imaging system (Bio-Rad Laboratories, Inc., Hercules, CA, USA). Quantification of proteins was conducted using Image J software (Version 1.52a; National Institute of Health, Bethesda, MD, USA), where protein densitometry was expressed relative to the densitometry of the corresponding GAPDH respectively.

2.16 Echocardiographic assessment of cardiac function

At the end-point of the experiment, myocardial function and cardiac dynamics were investigated by ultra-high frequency ultrasound for small animals (Vevo 3100 Preclinical Imaging System, FujiFilm VisualSonics, Canada) using the MicroScan Transducer MX550D (32-55MHz, Centre Transmit 40 MHz, Axial Resolution 40 µm) as previously described[47,48]. The Biomedical Sciences Institute Singapore Institutional Animal Care Committee approved all experiments. Mice were anesthetized with 1-2% isoflurane via mask and placed in supine position on a warming pad with integrated electrodes for continuous ECG monitoring (N=10 in each experimental group). Echocardiographic assessments of cardiac function were done in the morning and the IF mice were not fed prior to the experiments. Body temperature was monitored via a rectal temperature probe. After the complete removal of the hairs (hair removal cream), warmed up ultrasound gel was spread on the chest to avoid the formation of air bubbles and to ensure optimal sound quality. If needed, isoflurane was adjusted during the acquisition to maintain a relatively constant heart rate of over 300 beats per min (bmp). Two-dimensional and M-Mode were acquired in long and short axis using ECG-triggered image acquisition to assess ejection fraction, fractional shortening, cardiac output, stroke volume, and ventricular dimensions. The average values obtained from the long and short axis acquisitions were considered for all parameters. Strain analysis was performed on the long axis to measure the global longitudinal strain (GLS), strain rate, and radial strain[49]. Pulsed wave (PW) Doppler was used to measure the velocity of blood flow through the aortic, pulmonary, mitral, and tricuspidal valves. Septal mitral annular velocity was measured using tissue doppler echocardiography. To uncover a potential cardiac functional reserve, dobutamine-induced stress was performed after basal parameter acquisition. Dobutamine was administrated intraperitoneally in a single injection at 20 mg/kg. After the maximum increase in heart rate (generally within 4-5 min), two-dimensional and M-Mode acquisitions in long and short axes were repeated to assess ejection fraction, fractional shortening, cardiac output, stroke volume, ventricular dimensions, and strain in stress conditions.

2.17 Statistics

For physiological measurements such as fasting blood glucose, ketone levels and body weights, values are indicated as mean ± SEM (n = 20 mice/group). Significance is based on one-way ANOVA with Tukey's *post-hoc* test. P-value < 0.05 was considered statistically significant. The statistics for these comparisons were conducted using the GraphPad Prism software programme. For transcriptome data, differential expression analysis of the quantified transcripts was performed using DESeq R Package v.1.10.1. To control for false discovery rate (FDR), the resulting p values obtained by the Wald test were adjusted to q-values (multiple testing) using the Benjamini and Hochberg's method. Those transcripts with q-value < 0.05 were considered to be significantly differentially expressed among the different categories. For these significant genes, functional enrichment based on GO terms and associated KEGG pathways were inferred based on adjusted p-values < 0.05 as implemented in KOBAS. For proteome and phosphoproteome analyses, all peptide and protein identifications together with their modifications (phosphosites) were performed at FDR < 0.01 as implemented in Proteome Discoverer 2.2 (for proteome) and MaxQuant version 1.6.0.1 (for phosphoproteome). For TMT-based proteome data, biological replicates from the two TMT sets were combined following normalization and subjected to one-way analysis of variance (ANOVA) with Dunnett's *post hoc* test (multiple comparisons to control) at adjusted p-value < 0.01 for pairwise significance testing against AL control group to correct for multiple testing. The statistical analyses were implemented in R statistical environment. For functional enrichment analyses using proteome data, Fisher's exact test was implemented, and enriched categories were identified at FDR ≤ 0.05. 1-D and 2-D annotation enrichment for the proteome profiles to assess the distribution of specific functional groups among the different IF categories were performed using Perseus and controlled for FDR at an adjusted p-value < 0.05. For extracting differentially altered phosphorylation sites between the different groups, one-way ANOVA followed by Dunnett's *post-hoc* (multiple comparisons to control) was carried out and significantly altered sites were identified at adjusted p-value ≤ 0.05 to correct for multiple testing (implemented in R statistical environment). For immunoblot and echocardiographic analysis, all statistical analyses were conducted using the GraphPad Prism software programme. Data are presented as mean ± standard deviation for the indicated number of experiments. The difference in means between two columns was evaluated using the two-tailed unpaired Student's *t*-test (for two columns) or one-way ANOVA with Tukey's *post-hoc* test (for multiple comparisons to control). A p-value of less than 0.05 was considered statistically significant.

3. Results

Male C57BL/6 mice were fed a normal chow diet comprised of a caloric basis of 58%, 24%, and 18% carbohydrate, protein, and fat, respectively. Mice were randomly assigned to AL, daily IF12, IF16, or EOD schedules beginning at 3 months of age. The study design, including the timing of experimental interventions and blood and tissue collections, is summarized in **Supplementary Fig. 1**. To determine the extent to which IF affects energy metabolism, we measured the blood glucose and ketone levels, and body weight of all mice during the six-month dietary intervention period. Mice in the AL group exhibited a trend toward increased blood glucose levels at 3 and 6 months. In contrast, mice in the EOD group exhibited a large and highly significant decrease in blood glucose levels throughout the duration of the study (**Supplementary Fig. 1b**). Mice in the IF12 and IF16 groups exhibited glucose levels intermediate to the AL and EOD groups (**Supplementary Fig. 1b**). Ketone levels also displayed variability across different fasting regimens. On fasting days, mice in the EOD group exhibited blood ketone levels that were 3-fold greater than mice in the AL group. Ketone levels in mice in the IF16 and IF12 groups tended to be higher than those in the AL group but were substantially lower than in the EOD group. Notably, all IF and EOD animals exhibited significantly lower body weight than AL mice (**Supplementary Fig. 1c**). However, despite the differences in the fasting regimen pattern, we did not observe any difference in overall body weight between the IF and EOD groups (**Supplementary Fig. 1c**). Furthermore, no significant difference in the overall energy intake or compositional intake is observed across mice subjected to IF groups compared to the AL group (**Supplementary Fig. 1d**).

3.1 IF modifies the heart proteome

To obtain a comprehensive perspective of the mechanisms impacted by IF in heart, we carried out proteome profiling of heart tissues from at least four biological replicates comprising each dietary group (AL=4, IF12=5, IF16=5, EOD=4). The AL group served as a control to compare proteomic alterations across different IF regimens. Using tandem mass tag (TMT)-based high resolution liquid chromatography-mass spectrometry (LC-MS) analysis, we identified a total of 6,972 proteins (**Table S1**). Among the 5,578 proteins quantified across all the samples, 9% of the proteins were differentially expressed among the heart tissues from different dietary regimens compared to the control AL group (Dunnett adjusted p-value = 0.01, **Table S2**). Among these, only 60 proteins consistently overlapped with altered protein levels across all fasting regimens and were primarily involved in processes associated with

glycogen catabolism, fatty acid oxidation, and glycolysis (**Supplementary Fig. 2a**). In comparison with IF12, the proteomes were modulated to a greater extent in the longer fasting durations, IF16 and EOD. The EOD group exhibited the most significant number of protein abundance changes, with 44% modulations exclusively occurring within this group, including apolipoproteins that are important determinants of a healthy heart[50]. Approximately one-third of the differentially expressed proteins in IF groups compared to AL were enzymes with catalytic activity involved in energy homeostasis pathways. In addition to the expected fatty acid metabolism and glycolytic pathways, we observed enzymes involved in hypoxia, oxidative phosphorylation, bile acid metabolism, mTOR signaling, and myogenesis to be modulated with IF (**Supplementary Fig. 2b)**. We observed that most of the enzymes involved in glycolysis, including the rate-limiting enzyme phosphofructokinase (PFKFKB1/2) displayed decreased expression with IF except for hexokinase 1 (HK1), indicative of suppression of glycolysis (**Table S2**). Conversely, the expression of phosphoenolpyruvate carboxykinase (PCK2), which is involved in gluconeogenesis, was enhanced by IF.

Unsupervised hierarchical clustering of the altered heart proteome revealed that IF12, IF16, and EOD mice had different overall protein expression patterns and co-expressed protein clusters compared to mice in the AL group (**Fig. 1a).** Unlike clusters in IF16 and IF12 groups, which exhibited modest differences compared to the AL group, a distinct class of proteins showed increased abundance only in the EOD group. These clusters of proteins with exclusive upregulation in the EOD (FDR < 0.05) group belonged to processes such as mRNA processing, fatty acid metabolism, autophagy, and stress response mechanisms. Other processes such as cholesterol transport and phospholipid efflux showed a downward trend in the EOD group. Several other metabolic processes, including oxidative phosphorylation, amine catabolism, and fatty acid oxidation, were overall reduced in all IF groups compared to AL. We also observed distinct modulations of several kinases in a regimen-specific manner, with majority of the alterations occurring only with IF16 and EOD (**Supplementary Fig. 2c)**. Several of the kinases involved in the regulation of key metabolic pathways, such as glycolysis, exhibited decreased abundance in comparison with the AL group (**Fig. 1b**). With EOD, major determinants of insulin sensitivity such as AKT1 and mTOR were highly expressed, and several other stress-activated kinases MAPK9 and MAPK10, showed reduced abundance **(Fig. 1b and Supplementary Fig. 2c**).

To understand the molecular events accompanying each IF regimen, we performed 1-D annotation enrichment[51] identifying processes enriched at higher and lower protein abundances **(Fig. 1c and Table S3).** We observed upregulation of structural proteins involved processes such as focal adhesion and cell adhesion across all fasting regimens suggesting possible re-organization of the extracellular matrix interaction in heart tissues with IF. In addition, proteins regulating lipid kinase activity were observed in higher abundance in the hearts of mice from all three IF regimens compared to AL. We also observed specific signaling pathways to be selectively enriched in one IF regimen compared to the other IF regimens. For example, the IF12 group showed enrichment of proteins associated with cyclase activity, while the IF16 group displayed elevation of ERK signaling proteins. Signaling pathways involving the second messenger cAMP, however, were activated only with longer periods of fasting. This supports the notion that different IF regimens differentially modulate protein expression changes in the heart and impact signaling rewiring (**Fig. 1c and Table S3**). Apart from components of lipid metabolism and transport that were reduced across all IF groups, our data also showed that branched-chain amino acid (BCAA) metabolism, which is known to regulate several anabolic and catabolic cellular cascades[52], was significantly lower in all IF groups compared to the AL group (**Fig. 1c**).

3.2 Regimen-specific modulation of heart functional processes

The distinct and overlapping proteomic profiles for the three IF regimens suggested a progressive molecular and cellular remodeling of the heart in response to increasing fasting durations. While the overall metabolic responses were modulated across all regimens in comparison with AL, we further probed into regimen-specific differences to understand selective processes that were rewired with an increase in fasting duration (**Fig 2a-c**). Compared to AL, IF12 enhanced the processes that maintain the structural integrity of the heart, such as adhesion, extracellular structure, and cytoskeletal organization (**Fig. 2a**). We also observed increased expression of proteins involved in the immune and stress response, and endocytosis and exocytosis events in IF12. Along with significant changes to the circulatory process, which displayed increased protein abundances, protein networks associated with heart rate regulation were also altered by IF12. As expected, proteins involved in metabolic processes such as sterol metabolism and transport, glucose utilization, and protein synthesis were downregulated (**Fig. 2a**). While the protein trafficking network was enhanced in IF16, other immune functional networks (NF-κB and Wnt signaling, innate immune response, and T cell receptor signaling) and amino acid biosynthetic processes were

downregulated in IF16 in comparison with IF12 (**Fig. 2b**). Prolonged activation of NF-κB in immune cells occurs in several major cardiovascular diseases, including cardiac hypertrophy and heart failure, and aberrant Wnt signaling contributes to cardiac hypertrophy[53,54]. Changes in ion homeostasis and cardiac morphogenesis networks were also evident with an increase in fasting duration from IF12 to IF16. EOD introduced a wide spectrum of changes in the heart proteome. In addition to metabolic changes commonly, EOD led to epigenetic changes compared to IF16 (**Fig. 2c**). Proteins associated with chromatin remodeling and organization, and those involved in histone and other protein modifications showed increased abundance. In parallel, proteins that regulate transcription initiation and termination, transcript splicing, and nuclear import were also upregulated in the hearts of EOD mice. Also, an increase in the mitotic and nuclear division regulatory networks was observed. This starkly contrasted to reductions in cell cycle-related pathways observed specifically in IF12 or IF16 groups. Additionally, DNA repair and organelle assembly protein networks were upregulated by EOD. Along with reduced immune response and ion and sterol transport, EOD exhibited a reduced abundance of components involved in mitochondrial electron transport chain (ETC), pyruvate metabolism, and ATP generation compared to IF16 mice (**Fig. 2c**). EOD fasting also downregulated blood coagulation which may be crucial to reducing risk of pathological clot formation.

3.3 Post-transcriptional buffering of IF-responsive proteins

While we established that IF impacts the heart proteome and relays a regimen-specific effect on the expression patterns of proteins, we next investigated the transcriptome to probe IF-induced effects. For this, we performed RNA-seq based transcriptome profiling for heart tissues obtained from mice in different IF regimens (**Supplementary Fig. 3 and Table S4**). We obtained corresponding transcript readouts using RNA sequencing for approximately 93% of the proteins that were quantified across the different regimens. Comparison of correlation across transcripts and proteins abundance across the different groups revealed only a modest correlation as expected (Pearson correlation coefficient ~0.47) (**Supplementary Fig. 4a**), ruling out any regimen-specific differences. We next performed 2-D enrichment analyses to reveal correlated and non-correlated functional processes at the proteome and transcriptome levels (**Table S5**). This revealed that structural processes such as ECM-receptor interaction and metabolic pathways involving BCAA degradation showed consistent changes in proteome and transcriptome with IF (**Fig. 2d and Supplementary Fig. 4b**). Nevertheless, with increased fasting hours, mainly in the EOD group, we observed a trend shift in the

direction of proteome and transcriptome abundances **(Fig. 2d)**. Metabolic processes associated with fatty acid oxidation and monocarboxylic acid catabolic processes and immune processes related to autoimmunity and chemokine signaling showed the most noticeable drifts. On investigating the fatty acid oxidation cluster, we noticed that many of the key enzymes involved in the beta-oxidation of unsaturated (ECI1/2) and long-chain (or very long-chain) fatty acids (HADHA/B and ACADVL) showed differential transcript and protein abundances suggesting plausible buffering of protein levels beyond transcriptional regulation with IF. In comparing the enzyme abundances (**Supplementary Fig. 4c**), we found that some enzymes showed conserved correlation across different IF groups implying concerted rewiring of both transcriptome and proteome **(Supplementary Fig. 4c, Tables S2, and S4)**. Phospholipid phosphatase 1 (PLPP1) which is involved in the synthesis of glycerolipids and lipid uptake showed a dramatic decrease in protein abundance in the EOD group despite a modest increase in the corresponding transcript abundance. N-acetyltransferase NAT10 involved in histone acetylation and chromatin organization, ribonuclease RNASE4 participating in mRNA cleavage, and spliceosome-associated protein CWC27 involved in mRNA splicing all showed an exclusive increase only in the protein level with no observed changes in the mRNA level. Changes in these proteins were more obvious in the EOD group, and this supports extensive gene regulatory rewiring with extended fasting duration. Such discordant expression patterns at the mRNA and protein level could arise from post-transcriptional buffering that could potentially impact enzymes and kinases abundance and functions via post-translational modifications affecting protein stability or allosteric regulations that can alter activity.

With changes in metabolism closely linked to and regulated by circadian clocks, we assessed if time-restricted feeding regimens of IF12 and IF16 mice during the day (light phase) displayed any altered circadian patterns compared to AL or EOD mice by analyzing expression changes of core clock components at both the transcript and the protein levels (**Supplementary Fig. 5**). This analysis showed a differential expression profile of most clock gene transcripts compared with the AL control group irrespective of the fasting regimen pattern (**Table S4**). Notably, both the IF12 and IF16 groups were similar to the EOD fasting group despite the time-restricted feeding during daytime. Except for the transcripts of CRY1 and NR1D1 that showed differential expression between IF12 and EOD groups, all other clock gene transcripts showed consistent expression patterns across the three IF groups. In the corresponding proteome data, we only reliably quantified two clock components, CLOCK,

and CRY1, neither of which showed significant differential protein expression among the fasting regimens.

3.4 Time-resolved protein network remodeling during IF

To elucidate how functional protein networks are remodeled in response to IF, we curated protein-protein interactions (PPI) of all IF-responsive proteins and explored their functional crosstalk (**Fig. 3, Supplementary Fig. 6 and Table S6)**. Since many of the altered proteins were enzymes, we also considered functional interactions such as those that regulate gene expression, mediate enzymatic cascades or regulate protein phosphorylation in addition to physical interactions. To this end, we used the Pathway Commons database, a compendium of pathway-centric biologically relevant interactions[43], and mapped interactions for 441 (81%) of the IF-responsive proteins. To infer duration-specific effects, we specifically marked those proteins that were first altered with shorter fasting duration and those that appeared with longer fasting hours, such as IF16 or EOD (**Fig. 3a**). Changes in around 79 proteins appeared early within the IF12 regimen and some of these alterations were conserved until longer fasting durations at both IF16 and EOD (**Table S6**). Highly populated network clusters exclusively emerged with EOD that contributed to 189 proteins in the overall IF-modulated network (**Fig. 3a**), suggesting enhanced network rewiring with longer fasting duration.

We next performed a cluster assessment using the Cluster ONE graph-clustering algorithm[44] to identify densely connected network regions that may be functionally relevant. This highlighted several tightly connected clusters that included proteins responsive to different IF regimens and showed functional preference for specific metabolic processes **(Fig. 3b, Supplementary Fig. 7, and Table S6)**. The cluster that constituted proteins associated with fatty acid beta-oxidation and PPAR was the most highly enriched cluster exemplifying the impact of IF on lipid oxidation. It was evident that many of the proteins associated with this cluster tend to be downregulated during IF, particularly in EOD, except for a few proteins such as ACOT1, ACOT2, and EHHADH that showed high abundances exclusively with EOD **(Fig. 3b)**. Indeed, cardioprotective roles have been attributed to the fatty acyl-CoA thioesterase ACOT1 via its activation of PPARα/PGC1α signaling[55]. Another lipid metabolism-associated cluster impacted by IF12, IF16, and more by EOD, included proteins involved in cholesterol efflux, triglyceride homeostasis, and chylomicron clearance (**Fig. 3b**). The most prominent effects of IF on lipid metabolism were on the apolipoproteins APOA1/4, APOE, and APOC1/2/3, all of which declined in the EOD group. An increase in the level of

NPC2, an intracellular transporter mediating the export of cholesterol from lysosomes[56], was observed in the EOD group. PLTP, the increased activity of which is known to be associated with atherosclerosis, systolic dysfunction, obesity, and diabetes[57], was observed to be suppressed explicitly in all three IF groups.

Apart from these lipid-linked clusters, we also observed other clusters differentially modulated in an IF group-dependent manner. Signal transduction primarily via the insulin receptor and MAPK pathways emerged as one of the prominent clusters primarily comprising proteins modulated with longer fasting duration (**Fig. 3b**). B2M, a risk marker for cardiovascular disease[58], was found within this cluster. The network comprising RNA processing and splicing proteins mostly constituted proteins changing with EOD (**Supplementary Fig. 6 and Table S6**). The cluster with proteins involved in ubiquitination and proteolytic processes exhibited mostly included proteins altered with IF16. Upregulated by IF16 within this cluster was LNPEP, a zinc-dependent aminopeptidase that cleaves several peptide hormones and also catalyzes the conversion of angiotensinogen to cardioprotective angiotensin IV (AT4)[59,60]. From the network, we infer that other metabolic processes such as pyruvate and amino acid metabolism and glycolysis show gradual modulations in protein abundance with increasing fasting duration (IF12 < IF16 < EOD) (**Supplementary Fig. 6**). Further, based on their centrality, we inferred kinases including AKT1, CDC42, PKM, EGFR, and CSNK2A1 as IF-responsive hubs that effectively relay signaling modulations during IF-induced network rewiring.

To determine how the IF-induced network rewiring impacts downstream transcriptional programs, we assessed transcription factors enriched at each IF regimen using ChIP enrichment analysis (ChEA) database (**Fig. 3c**). Several key transcription factors with metabolic relevance including PPARα/γ, FOXA1/2, NUCKS1, HNF4A among others were found to be enriched. While some such as ELKF, TAF7L, and PPARα were modulated irrespective of the IF regimen, others, including HOXC9, YY1, and JARID1A showed exclusive enrichment in the EOD group.

3.5 Modified protein co-regulation in heart during IF

Dynamic interactions among proteins coordinate cellular homeostasis and adaptive responses to environmental challenges. To decipher the effects of IF on such protein associations, we investigated the protein co-regulation network of heart proteome for IF regimen-specific

perturbations using the 'interactome mapping by high-throughput quantitative proteome analysis' (IMAHP) method[46,61]. The correlation network comprised 44,966 associating protein pairs, of which a majority (34,629 pairs) involved positive co-regulations between the associated proteins **(Supplementary Fig. 8 and Table S7a-b)**. To identify protein associations perturbed in an IF group-dependent manner, we carried out an outlier analysis to specifically derive associations that displayed significant deviation from the overall correlation across all co-regulated proteins. This revealed higher deviations by ~40% across all IF groups than the AL group, suggestive of dynamic modulation of protein associations with IF. We identified consensus proteins that were consistently altered in protein associations across the different IF regimens (p-value < 0.05) **(Supplementary Fig. 8 and Table S7c)** and accordingly identified the greatest number of affected proteins in the IF16 and EOD groups, with the EOD group showing exclusive changes in 118 proteins and the IF16 group with 69 altered proteins. The IF12 group displayed only a small number of perturbed associations similar to the AL group. Also, we noticed that many protein associations affected by IF16 were similarly affected by EOD fasting. Proteins with perturbations in the AL group preferred metabolic processes, including carbohydrate and glycogen metabolism, oxidation-reduction, and protein transport **(Supplementary Fig. 8 and Table 7c)**. Among these were phosphofructokinase (PFKL), lactate dehydrogenase A (LDHA), phosphoglycerate dehydrogenase (PHGDH), and kinases AKT2 and DTYMK. Unlike AKT1, which was found to be upregulated by IF, AKT2 did not vary in abundance with any IF regimen. Proteins with association perturbations in IF12 regimen mainly were localized to the mitochondria and showed an inclination towards oxidative stress mechanisms. The IF16 regimen impacted proteins in various cellular processes, including platelet activation, migration, translational control, fatty acid oxidation, and Rap1 signaling. Several association modulations involved integrins, myosin, and actin, including ITGB3 and ITGA2B, which have been linked to cardiac pathologies[62]. While perturbations accompanying extended EOD fasting maintained some of the functional changes evident in IF16 hearts, such as NADH oxidation and electron transport chain, association alterations also occurred in lipid-related pathways. Importantly, we observed modulation of the PPAR signaling pathway by EOD fasting with key components PDPK1, APOA1, FABP3, PCK2, and SCP2 affected **(Supplementary Fig. 8b)**. This finding is interesting as PPAR modulators are currently being evaluated as therapeutic players for several cardiac diseases[63].

A consistent pattern across the inferred association perturbations was that most of these involved proteins in the metabolic pathways were also localized to the mitochondria **(Supplementary Fig. 9a)**. We constructed a mitochondrial association network to identify the modulated associations that occurred in an IF regimen-specific manner. From the network, it was evident that many of the perturbed proteins co-associate, particularly in the EOD group, and share associations relevant to an intricate orchestration of mitochondrial functional protein associations in response to IF **(Supplementary Fig. 9b and Table S7d)**. Among the mitochondrial proteins affected by IF, some, including UQCRC1, METAP1D, SCP2, COA7, AFG3L2, FAM162A, and COA4, were involved in associations spanning multiple functional processes suggesting coordinating rewiring of various pathways by mitochondrial functions. For instance, UQCRC1 shares IF responsivity with proteins involved in both fatty acid oxidation and carbohydrate metabolism. Overall, our data suggest the involvement of mitochondrial proteins in adaptive responses of the heart to IF.

3.6 IF impacts phosphosignaling pathways in a cardioprotective manner

To gain deeper insight into IF-induced signaling alterations in myocardial cells, we investigated changes in the phosphorylation landscape that accompanies IF **(Fig. 4, Supplementary Fig. 10, and Table S8a)**. We enriched phosphopeptides from heart tissue homogenates (n=3 from each group) and then profiled them using label-free phosphoproteome analysis. Among the different groups, we identified 12,540 phosphorylated sites on 2,931 proteins of which, ~80% and ~19% sites were phosphorylated on serine and threonine respectively, with only 1% being tyrosine phosphorylated. Peptides with single phosphorylation sites represented 81% of the phosphopeptides analyzed. Among the sites identified, 66% corresponded with those curated in the PhosphoSitePlus database[64]. There was high reproducibility of phosphopeptide quantifications among the biological replicates with an average intensity correlation of 0.86.

To elucidate IF-induced changes in protein phosphorylation, we focused on 6,935 unique phosphorylation sites from 7615 phosphopeptides that were quantified from at least two biological replicates in the dietary groups (**Table S8b**). Approximately 84% of these belonged to class I phosphorylation sites with a localization probability ≥ 0.75, and overall displayed an average localization probability of 0.90, indicative of high phosphosite confidence. On assessing those sites that were significantly altered (Dunnett adjusted p-value < 0.05) with IF, we observed that phosphorylation changes varied with increasing duration of the fasting

period with EOD exhibiting the greatest number of phosphosite abundance changes, similar to what was observed in the proteome (**Fig. 4a** and **Table S8b**). However, in contrast to proteome remodeling, phosphoproteome profiling revealed increased phosphosite abundance on a majority of the differentially modulated phosphoproteins, and several of these were independent of proteome changes. This is intriguing as it points to differential exploitation of translational and post-translational mechanisms to remodel cardiac cells in response to IF. Site-specific phosphorylation changes occurred on several proteins involved in structural remodeling of the heart, such as titin, which was observed with multiple changes (**Fig. 4a),** and on regulatory proteins, including kinases, phosphatases, and enzymes in metabolic pathways (**Supplementary Fig. 10)**. For instance, phosphorylation changes were observed on several MAPK associated kinases including MAPK1/3 and MAPK12, PKC family kinases including PKC-alpha, -beta, and -theta kinases that coordinate muscle contraction, including MYLK, MYLK3, and PAK2, and sphingolipid signaling kinase SPHK2 (**Table S8b**). Enzymes involved in lipid metabolism such as ACOT1 and ACSL1, glycolytic enzyme triose phosphate isomerase (TPI1) and fumarate hydratase (FH) in the TCA cycle, phosphorylase kinase (PHKB) involved in glycogen breakdown, all showed IF-responsive changes in phosphosite abundance emphasizing phosphorylation-dependent remodeling of energy homeostasis pathways with IF.

While phosphorylation signatures reflect kinase activities, we noticed that only 2.8% of the phosphosites we quantified had experimentally validated kinases. Hence, we defined kinase-substrate relationships through motif mapping for each IF regimen. Accordingly, we focused on all the modulated phosphosites and identified motifs specifically enriched (p-value < 0.05) within distinct phosphosite expression clusters. The clustering revealed discrete patterns of phosphorylation changes that occur in response to each IF regimen (**Fig. 4b**). PKA/PKC were commonly activated across all IF regimens. CSNK and p38 signaling were exclusive to the IF16 group, while AMPK, the master regulator of energy metabolism, exhibited activation in longer fasting groups. Overall, the kinase activation profiles were more pronounced in IF16 and EOD groups compared to the AL group. Pathway-based assessment of the modulated phosphoproteins highlighted the conserved modulation of pathways associated with insulin signaling, focal adhesion, and cGMP-PKG signaling across all IF groups (**Fig. 4c-d**). cGMP-PKG signaling is known to mediate vasorelaxation, and activation of this pathway is regarded as cardioprotective[65]. In line with the kinase prediction, components of AMPK signaling showed significant modulation in both IF16 and EOD groups (**Fig. 4c-d**). In summary, our

phosphoproteome analyses revealed that IF impacts different signaling pathways that influence the heart's structural and functional plasticity.

To further validate our proteomics data, we carried out immunoblot validation to confirm a few key findings we inferred based on IF-induced proteome and phosphoproteome alterations. For this and subsequent functional studies, we chose the IF16 group as it showed IF-specific rewiring of several kinase-induced pathway rewiring events and is also a more realistic fasting regimen in human. We evaluated the expression levels of selected proteins from various pathways, namely p-AMPKα/AMPKα, PKG-1, MYPT1, PPARγ, p-GSKαβ/GSKαβ, AKT, Insulin receptor β, and p-IRS1/IRS-1, in IF16 and AL using immunoblotting (**Fig. 5a-b**). In line with our proteomic inferences, compared to the AL group, expression levels of pAMPK/AMPK, PPARγ, MYPT1 and IRS1 were significantly higher in the IF16 group. In addition, we observed increasing trends of PKG-1, AKT and decreasing trend of p-GSKαβ/GSKαβ in the IF16 group compared to the AL group (**Fig. 5a-b**). Overall, these results further support the findings of IF-modulated pathways observed from our omics analyses.

3.7 IF improves cardiac performance after stress

With the enhanced cardiac resilience inferred from the omics data, we next investigated the effects of IF on heart function and dynamics in the IF mice compared to the AL mice. For this, we performed echocardiographic measurements in mice that had been maintained on AL or IF16 diets for 6 months. While no differences in heart function were observed between IF and AL groups, AL mice started to show signs of age deterioration, such as prolonged E/A and shortened deceleration time[66] (**Supplementary Fig. 11, Supplementary videos 1-4**). To evaluate cardiac functional reserve, dobutamine stress tests were performed after basal parameter acquisition. As expected, administration of dobutamine resulted in significant inotropic, lusitropic, and chronotropic cardiac responses[48] in both groups. However, the increase in heart rate, as well as ejection fraction, fractional shortening and left ventricular dimensions after stress were significantly higher in IF16 mice compared with AL control mice (**Table S9**, **Fig. 6a, Supplementary videos 1-4**), suggesting that IF preserves myocardial functional reserve. To confirm these findings, strain analyses were performed. Longitudinal and radial strain significantly improved after dobutamine administration in IF16

mice but not in AL mice, suggesting that IF preserved systolic contractile reserve, which deteriorated with age in the AL mice (**Table S9, Figure 6b**).

4. Discussion

Increasing evidence from animal and human studies suggests that IF reduces the risk for cardiovascular disease and bolsters myocardial function and resilience[3,67,68]. However, except for enhancement of parasympathetic tone[4,69] and upregulation of protein chaperones[70], the underlying mechanisms are unknown. Collectively, our comprehensive datasets provide a window into the molecular, cellular, structural, and functional remodeling of the heart in mice adapted to IF eating patterns. To address the question of how the duration of the fasting period in specific IF regimens affects the molecular remodeling of the heart, we compared the molecular effects of IF12, IF16, and EOD fasting. All three IF regimens affected the pathways that regulate cellular carbohydrate, lipid and protein metabolism, cell-cell interactions, and myocardial cell contractility. Previous findings suggested that the beneficial effects of IF on organ function and stress resistance require 2-4 weeks to be fully engaged[4,24,71,72]. If and to what extent the molecular remodeling of the heart in response to IF reverts to the pre-IF state upon return to ad libitum feeding remains to be determined.

There are many similarities in the effects of aerobic exercise and IF on the cardiovascular system that beg the question of the extent of overlap in the underlying molecular mechanisms. For example, both IF and regular exercise training increase parasympathetic tone and heart rate variability, and both can protect the myocardium against ischemic injury[73,74]. Moreover, both exercise and IF stimulate mitochondrial biogenesis in skeletal muscle[16,75]. Exercise training also stimulates mitochondrial biogenesis in myocardial cells[76]. Studies of the effects of IF on the brain and skeletal muscle suggest that IF activates several major pathways engaged by ischemic and metabolic preconditioning, including upregulation of protein chaperones, anti-apoptotic proteins, and autophagy, and suppression of the mTOR pathway and protein synthesis[16,17]. Previous research has led to the development of several treatments that mimic one or more effects of exercise, caloric restriction, and IF. Examples include agents that induce mild transient metabolic stress such as 2-deoxyglucose and mitochondrial uncoupling agents[6,24,77-79], ketone esters[80,81,] and mTOR inhibitors such as rapamycin[82].

Our analysis of functional interactions and IF-induced alterations provides a global view of molecular and metabolic rewiring influencing various aspects of cardiac performance and bioenergetics. We observed IF-induced changes in expression of several enzymes functioning in key energy pathways, as well as kinases involved in cellular signaling. While IF triggered the downregulation of several lipid metabolism enzymes, thioesterases that regulate fatty acid flux, such as ACOT1, ACOT2, and ACOT7, were upregulated, especially in the EOD group. ACOT1, for instance, functions as a molecular rheostat to impede excessive fatty acid oxidation during fasting and dampens associated inflammation and oxidative stress by inducing protective PPARα signaling[83]. Such an induction of PPARα activity with IF is indeed supported by increased protein abundance of several of its transcriptional targets, including HMGCS2 and PDK4. It is noteworthy that signaling alterations driving such PPAR-associated modulations were also evident from IF-induced phosphorylation changes, including activation of PKA, one of the key modulators of PPAR transcriptional activity, especially in the context of lipid oxidation during fasting and exercise[84]. In addition to modulating fatty acid flux, PKA also triggers glycogen breakdown by activating phosphorylase kinase PHKB, which in turn triggers glycogen phosphorylase to release glucose 1 phosphate from glycogen[85]. Our data point to an increase in phosphorylation site abundance on PHKB with IF suggesting increased turnover of glycogen with IF. The PKA effect of IF was accompanied by changes in associated cAMP signaling which also showed enhanced activation with prolonged durations of fasting as indicated by proteome modulation. The cAMP/PKA axis plays crucial modulatory roles in various aspects of cardiac physiology, including cardiomyocyte contractility via excitation–contraction coupling (ECC), control of heart rate, and downstream relay of β-adrenergic receptor signaling, is known to be perturbed in instances of heart failure[86-88].

AMPK emerged as another prominent signaling cascade that was activated with longer hours of fasting (IF16 and beyond) based on the modulated phosphorylation sites. We observed that the substrates of AMPK were associated with multiple aspects of energy usage that are known to enhance the metabolic flexibility of the heart. TBC1D1, another substrate that is important in AMPK-induced GLUT4 translocation, also showed a consistent increase in functional phosphorylation with increasing fasting duration[89]. Disruption of GLUT4 trafficking is associated with impaired glucose uptake and ensuing insulin resistance[90], and the phosphorylation change on TBC1D1 and GLUT4 along with the predicted increase in AKT activity suggest that IF improves insulin sensitivity in the heart by modulating glucose uptake

and resetting aberrations in insulin signaling via increasing phosphorylation of such proteins. The effects of insulin signaling are primarily mediated by AKT. We identified AKT1 to be differentially expressed based on protein abundance, AKT2 to have specific alterations in IF triggered association modulations, and also predicted AKT to be induced based on substrate signatures from our phosphoproteome data. Collectively, our data suggest that AKT may be an important mediator of heart cell responses to IF. In addition, there was a striking increase in phosphorylation of epitopes on numerous proteins known to regulate heart development and cardiomyocyte contraction, particularly that is a crucial determinant of myocardial passive stiffness and whose malfunction is associated with various myopathies[91,92]. In all, these highlight varying degrees of kinase and metabolic rewiring in the heart induced by different durations of IF, with the most protective effects accompanying prolonged fasting.

Whilst our data provide a comprehensive molecular snapshot of the changes accompanying various courses of IF, there is a limitation that our landscape is reflective of net changes occurring across the entire heart. Thus, it is challenging to understand specific changes within the different cell types that comprise the heart. Such a limitation is exaggerated, particularly for the transcriptome analysis, as cardiomyocytes account for only 30% of cells in the mammalian heart and yet account for the majority of the cardiac mass[93]. Knowledge of cell type-specific responses to IF will therefore be important to delineate distinct responses of heart cells to various IF regimens, and future studies exploring single-cell sequencing will add new dimensions to our understanding of cardiac dynamics with IF.

Further experimentation with different aspects of our study is required for detailed understanding of our findings. The timing of fasting cycles in this study may not promote synchronization of the natural circadian rhythm of nocturnal rodents, which may impact the potential for translating these to other model systems and understanding human patho-physiology. It has been established that time-restricted feeding/intermittent fasting cycles impact and can reset secondary tissue-specific peripheral clocks independent of the master circadian clock that is generally phase-locked to light-dark cycles[94-96]. While such mechanisms have been well documented in the context of liver and hepatic clocks, the impact of feeding on cardiac clock rhythmicity, however, remains to be deciphered. Evidence from our data suggests that fasting regimens affect circadian oscillations in heart cells, at least in part, independently of the central light-dark cycle-responsive clock. In addition, our analysis of cardiac function only included the AL and IF16 groups. We selected the IF16 fasting

regimen to perform proof of principle functional experiments to further understand the functional outcome of proteomic changes observed. Echocardiographic analysis of the EOD group may provide significant information on the effect of IF as the EOD group had the largest effect sizes from multi-omics analyses. With our study highlighting several kinase rewiring and signaling pathways impacted by IF based on modulations in proteome and phosphorylation site modulations, it will be interesting to follow-up on several of these to further assess their functional significance in the context of heart health and function. It is noteworthy that previous studies established that the EOD regimen leads to hearts with thinner walls and a lower left ventricular end-diastolic volume (LVEDV)[20] and lower blood pressure and heart rate[5] than those of control animals. The latter effects of EOD were associated with cardioprotection in a rat model of myocardial infarction[20]. Furthermore, our multi-omics study was limited to mice 6 to 9 months old, and it is, therefore, difficult to draw conclusions as to the effects of IF on ageing heart functions. All three IF groups maintained similar average body weights throughout the study period and were significantly lower than the AL group. Therefore, the different transcriptomes, proteomes, and phosphoproteomics observed among the three IF groups were independent of body weight. Our data suggest overlapping but distinct molecular adaptations of the heart to different intermittent fasting regimens.

In conclusion, our comprehensive multi-omics analysis sheds light on the intricate molecular mechanisms underlying the beneficial effects of intermittent fasting (IF) on cardiac health and disease prevention. Our findings demonstrate that various IF regimens induce distinct and time-dependent changes in the cardiac proteome, with longer fasting periods resulting in more significant alterations. The EOD group, in particular, exhibited the most significant protein abundance changes. The unsupervised hierarchical clustering analysis of the altered heart proteome highlights unique protein expression patterns and co-expressed protein clusters in all IF groups compared to the AL group. Collectively, these results provide valuable insights into potential pharmacological targets for developing novel therapeutic strategies for cardiovascular diseases. Future studies may further explore these targets and the underlying pathways to advance the development of effective interventions to improve cardiac health.

Funding

This work was supported by ODPRT, National University of Singapore, National Medical Research Council Research Grants (NMRC-CBRG-0102/2016 and

NMRC/OFIRG/0036/2017), Singapore and Agency for Science, Technology and Research, Singapore and the start up fund from La Trobe University, Melbourne, Australia.

Acknowledgments

Published on a preprint server: bioRxiv 2021.03.04.433999; doi: https://doi.org/10.1101/2021.03.04.433999

Supplementary Fig. 1a in this article was created using BioRender.

Conflicts of interest

The authors declare that they have no conflict of interest.

Data availability

The mass spectrometry proteomics data have been deposited to the ProteomeXchange Consortium via the PRIDE partner repository with the dataset identifier PXD015452. The data can be accessed using Username**:** reviewer34563@ebi.ac.uk **Password:** Y3btQBCL. High-throughput RNA sequencing data from this manuscript have been submitted to the NCBI Sequence Read Archive (SRA) under accession number GSE133290.

Ethics approval

The National University of Singapore Animal Care and Use Committee approved all experimental procedures performed *in vivo*.

Author contributions

Study Conception & Design: T.V.A., and J.G; Investigation-Performed Experiment or Data Collection: T.V.A., A.A.S., E.A.L., J.K., H.L.F.S., D.T.Z.H., C.R., D.Y.W.F., L.P., D.C.M., G.Y.Q.N., J.K., S.H.B., K.M., M.G., Y.C., Y.C., and R.R.S; Computational & Statistical Analysis: A.A.S., T.V.A., and J.G; Data Interpretation & Biological Analysis: T.V.A., A.A.S., E.A.L., C.G.S., D.G.J., G.D., M.P.M., and J.G; Writing-Manuscript Preparation: T.V.A., A.A.S., E.A.L., J.G., H.L.F.S., C.G.S., M.G., K.M., M.P.M., D.G.J., G.R.D., R.R.S. and B.K.K; Supervision & Administration: T.V.A., and J.G.

References

1. Lahey R, Khan SS. Trends in Obesity and Risk of Cardiovascular Disease. *Curr Epidemiol Rep* 2018;**5**:243-251.
2. de Cabo R, Mattson MP. Effects of Intermittent Fasting on Health, Aging, and Disease. *N Engl J Med* 2019;**381**:2541-2551.
3. Mattson MP, Longo VD, Harvie M. Impact of intermittent fasting on health and disease processes. *Ageing Res Rev* 2017;**39**:46-58.
4. Mager DE, Wan R, Brown M, Cheng A, Wareski P, Abernethy DR, Mattson MP. Caloric restriction and intermittent fasting alter spectral measures of heart rate and blood pressure variability in rats. *FASEB J* 2006;**20**:631-637.
5. Wan R, Camandola S, Mattson MP. Intermittent fasting and dietary supplementation with 2-deoxy-D-glucose improve functional and metabolic cardiovascular risk factors in rats. *FASEB J* 2003;**17**:1133-1134.
6. Wan R, Camandola S, Mattson MP. Intermittent food deprivation improves cardiovascular and neuroendocrine responses to stress in rats. *J Nutr* 2003;**133**:1921-1929.
7. Wan R, Weigand LA, Bateman R, Griffioen K, Mendelowitz D, Mattson MP. Evidence that BDNF regulates heart rate by a mechanism involving increased brainstem parasympathetic neuron excitability. *J Neurochem* 2014;**129**:573-580.
8. Castello L, Maina M, Testa G, Cavallini G, Biasi F, Donati A, Leonarduzzi G, Bergamini E, Poli G, Chiarpotto E. Alternate-day fasting reverses the age-associated hypertrophy phenotype in rat heart by influencing the ERK and PI3K signaling pathways. *Mech Ageing Dev* 2011;**132**:305-314.
9. Harvie MN, Pegington M, Mattson MP, Frystyk J, Dillon B, Evans G, Cuzick J, Jebb SA, Martin B, Cutler RG, Son TG, Maudsley S, Carlson OD, Egan JM, Flyvbjerg A, Howell A. The effects of intermittent or continuous energy restriction on weight loss and metabolic disease risk markers: a randomized trial in young overweight women. *Int J Obes (Lond)* 2011;**35**:714-727.
10. Harvie M, Wright C, Pegington M, McMullan D, Mitchell E, Martin B, Cutler RG, Evans G, Whiteside S, Maudsley S, Camandola S, Wang R, Carlson OD, Egan JM, Mattson MP, Howell A. The effect of intermittent energy and carbohydrate restriction v. daily energy restriction on weight loss and metabolic disease risk markers in overweight women. *Br J Nutr* 2013;**110**:1534-1547.
11. Stein PK, Soare A, Meyer TE, Cangemi R, Holloszy JO, Fontana L. Caloric restriction may reverse age-related autonomic decline in humans. *Aging Cell* 2012;**11**:644-650.
12. Weiss EP, Fontana L. Caloric restriction: powerful protection for the aging heart and vasculature. *Am J Physiol Heart Circ Physiol* 2011;**301**:H1205-1219.
13. Stekovic S, Hofer SJ, Tripolt N, Aon MA, Royer P, Pein L, Stadler JT, Pendl T, Prietl B, Url J, Schroeder S, Tadic J, Eisenberg T, Magnes C, Stumpe M, Zuegner E, Bordag N, Riedl R, Schmidt A, Kolesnik E, Verheyen N, Springer A, Madl T, Sinner F, de Cabo R, Kroemer G, Obermayer-Pietsch B, Dengjel J, Sourij H, Pieber TR, Madeo F. Alternate Day Fasting Improves Physiological and Molecular Markers of Aging in Healthy, Non-obese Humans. *Cell Metab* 2019;**30**:462-476.e6.
14. Arumugam TV, Phillips TM, Cheng A, Morrell CH, Mattson MP, Wan R. Age and energy intake interact to modify cell stress pathways and stroke outcome. *Ann Neurol* 2010;**67**:41-52.
15. Kim J, Kang SW, Mallilankaraman K, Baik SH, Lim JC, Balaganapathy P, She DT, Lok KZ, Fann DY, Thambiayah U, Tang SC, Stranahan AM, Dheen ST, Gelderblom M, Seet RC, Karamyan VT, Vemuganti R, Sobey CG, Mattson MP, Jo DG, Arumugam

TV. Transcriptome analysis reveals intermittent fasting-induced genetic changes in ischemic stroke. *Hum Mol Genet* 2018;**27**:1497-1513.
16. Marosi K, Moehl K, Navas-Enamorado I, Mitchell SJ, Zhang Y, Lehrmann E, Aon MA, Cortassa S, Becker KG, Mattson MP. Metabolic and molecular framework for the enhancement of endurance by intermittent food deprivation. *FASEB J* 2018;**32**:3844-3858.
17. Mattson MP, Arumugam TV. Hallmarks of Brain Aging: Adaptive and Pathological Modification by Metabolic States. *Cell Metab* 2018;**27**:1176-1199.
18. Wan R, Ahmet I, Brown M, Cheng A, Kamimura N, Talan M, Mattson MP. Cardioprotective effect of intermittent fasting is associated with an elevation of adiponectin levels in rats. *J Nutr Biochem* 2010;**21**:413-417.
19. Ahmet I, Tae HJ, de Cabo R, Lakatta EG, Talan MI. Effects of calorie restriction on cardioprotection and cardiovascular health. *J Mol Cell Cardiol* 2011;**51**:263-271.
20. Ahmet I, Wan R, Mattson MP, Lakatta EG, Talan M. Cardioprotection by intermittent fasting in rats. *Circulation* 2005;**112**:3115-3121.
21. Godar RJ, Ma X, Liu H, Murphy JT, Weinheimer CJ, Kovacs A, Crosby SD, Saftig P, Diwan A. Repetitive stimulation of autophagy-lysosome machinery by intermittent fasting preconditions the myocardium to ischemia-reperfusion injury. *Autophagy* 2015;**11**:1537-1560.
22. Katare RG, Kakinuma Y, Arikawa M, Yamasaki F, Sato T. Chronic intermittent fasting improves the survival following large myocardial ischemia by activation of BDNF/VEGF/PI3K signaling pathway. *J Mol Cell Cardiol* 2009;**46**:405-412.
23. Cheng A, Yang Y, Zhou Y, Maharana C, Lu D, Peng W, Liu Y, Wan R, Marosi K, Misiak M, Bohr VA, Mattson MP. Mitochondrial SIRT3 Mediates Adaptive Responses of Neurons to Exercise and Metabolic and Excitatory Challenges. *Cell Metab* 2016;**23**:128-142.
24. Liu Y, Cheng A, Li YJ, Yang Y, Kishimoto Y, Zhang S, Wang Y, Wan R, Raefsky SM, Lu D, Saito T, Saido T, Zhu J, Wu LJ, Mattson MP. SIRT3 mediates hippocampal synaptic adaptations to intermittent fasting and ameliorates deficits in APP mutant mice. *Nat Commun* 2019;**10**:1886.
25. Marosi K, Kim SW, Moehl K, Scheibye-Knudsen M, Cheng A, Cutler R, Camandola S, Mattson MP. 3-Hydroxybutyrate regulates energy metabolism and induces BDNF expression in cerebral cortical neurons. *J Neurochem* 2016;**139**:769-781.
26. Newman JC, Verdin E. β-Hydroxybutyrate: A Signaling Metabolite. *Annu Rev Nutr* 2017;**37**:51-76.
27. Yudkoff M, Daikhin Y, Melø TM, Nissim I, Sonnewald U, Nissim I. The ketogenic diet and brain metabolism of amino acids: relationship to the anticonvulsant effect. *Annu Rev Nutr* 2007;**27**:415-430.
28. Ng GY, Kang SW, Kim J, Alli-Shaik A, Baik SH, Jo DG, Hande MP, Sobey CG, Gunaratne J, Fann DY, Arumugam TV. Genome-Wide Transcriptome Analysis Reveals Intermittent Fasting-Induced Metabolic Rewiring in the Liver. *Dose Response* 2019;**17**:1559325819876780.
29. Shaik AA, Qiu B, Wee S, Choi H, Gunaratne J, Tergaonkar V. Phosphoprotein network analysis of white adipose tissues unveils deregulated pathways in response to high-fat diet. *Sci Rep* 2016;**6**:25844.
30. Hatchwell L, Harney DJ, Cielesh M, Young K, Koay YC, O'Sullivan JF, Larance M. Multi-omics Analysis of the Intermittent Fasting Response in Mice Identifies an Unexpected Role for HNF4α. *Cell Rep* 2020;**30**:3566-3582.e4.

31. Sacco F, Seelig A, Humphrey SJ, Krahmer N, Volta F, Reggio A, Marchetti P, Gerdes J, Mann M. Phosphoproteomics Reveals the GSK3-PDX1 Axis as a Key Pathogenic Signaling Node in Diabetic Islets. *Cell Metab* 2019;**29**:1422-1432.e3.
32. Sacco F, Humphrey SJ, Cox J, Mischnik M, Schulte A, Klabunde T, Schäfer M, Mann M. Glucose-regulated and drug-perturbed phosphoproteome reveals molecular mechanisms controlling insulin secretion. *Nat Commun* 2016;**7**:13250.
33. Rappsilber J, Mann M, Ishihama Y. Protocol for micro-purification, enrichment, pre-fractionation and storage of peptides for proteomics using StageTips. *Nat Protoc* 2007;**2**:1896-1906.
34. Tyanova S, Temu T, Cox J. The MaxQuant computational platform for mass spectrometry-based shotgun proteomics. *Nat Protoc* 2016;**11**:2301-2319.
35. Cox J, Hein MY, Luber CA, Paron I, Nagaraj N, Mann M. Accurate proteome-wide label-free quantification by delayed normalization and maximal peptide ratio extraction, termed MaxLFQ. *Mol Cell Proteomics* 2014;**13**:2513-2526.
36. Tyanova S, Temu T, Sinitcyn P, Carlson A, Hein MY, Geiger T, Mann M, Cox J. The Perseus computational platform for comprehensive analysis of (prote)omics data. *Nat Methods* 2016;**13**:731-740.
37. Subramanian A, Tamayo P, Mootha VK, Mukherjee S, Ebert BL, Gillette MA, Paulovich A, Pomeroy SL, Golub TR, Lander ES, Mesirov JP. Gene set enrichment analysis: a knowledge-based approach for interpreting genome-wide expression profiles. *Proc Natl Acad Sci U S A* 2005;**102**:15545-15550.
38. Merico D, Isserlin R, Stueker O, Emili A, Bader GD. Enrichment map: a network-based method for gene-set enrichment visualization and interpretation. PLoS One 2010;**5**:e13984.
39. Plubell DL, Wilmarth PA, Zhao Y, Fenton AM, Minnier J, Reddy AP, Klimek J, Yang X, David LL, Pamir N. Extended Multiplexing of Tandem Mass Tags (TMT) Labeling Reveals Age and High Fat Diet Specific Proteome Changes in Mouse Epididymal Adipose Tissue. *Mol Cell Proteomics* 2017;**16**:873-890.
40. Kuleshov MV, Jones MR, Rouillard AD, Fernandez NF, Duan Q, Wang Z, Koplev S, Jenkins SL, Jagodnik KM, Lachmann A, McDermott MG, Monteiro CD, Gundersen GW, Ma'ayan A. Enrichr: a comprehensive gene set enrichment analysis web server 2016 update. *Nucleic Acids Res* 2016;**44**:W90-7.
41. Lachmann A, Xu H, Krishnan J, Berger SI, Mazloom AR, Ma'ayan A. ChEA: transcription factor regulation inferred from integrating genome-wide ChIP-X experiments. *Bioinformatics* 2010;**26**:2438-44.
42. Huang da W, Sherman BT, Lempicki RA. Systematic and integrative analysis of large gene lists using DAVID bioinformatics resources. *Nat Protoc* 2009;**4**:44-57.
43. Cerami EG, Gross BE, Demir E, Rodchenkov I, Babur O, Anwar N, Schultz N, Bader GD, Sander C. Pathway Commons, a web resource for biological pathway data. *Nucleic Acids Res* 2011;**39**:D685-690.
44. Nepusz T, Yu H, Paccanaro A. Detecting overlapping protein complexes in protein-protein interaction networks. *Nat Methods* 2012;**9**:471-472.
45. Shannon P, Markiel A, Ozier O, Baliga NS, Wang JT, Ramage D, Amin N, Schwikowski B, Ideker T. Cytoscape: a software environment for integrated models of biomolecular interaction networks. *Genome Res* 2003;**13**:2498-2504.
46. Lapek JD Jr, Greninger P, Morris R, Amzallag A, Pruteanu-Malinici I, Benes CH, Haas W. Detection of dysregulated protein-association networks by high-throughput proteomics predicts cancer vulnerabilities. *Nat Biotechnol* 2017;**35**:983-989.
47. Liehn EA, Kanzler I, Konschalla S, Kroh A, Simsekyilmaz S, Sönmez TT, Bucala R, Bernhagen J, Weber C. Compartmentalized protective and detrimental effects of

endogenous macrophage migration-inhibitory factor mediated by CXCR2 in a mouse model of myocardial ischemia/reperfusion. *Arterioscler Thromb Vasc Biol* 2013;**33**:2180-2186.
48. Tyrankiewicz U, Skorka T, Jablonska M, Petkow-Dimitrow P, Chlopicki S. Characterization of the cardiac response to a low and high dose of dobutamine in the mouse model of dilated cardiomyopathy by MRI in vivo. *J Magn Reson Imaging* 2013;**37**:669-677.
49. Lindsey ML, Kassiri Z, Virag JAI, de Castro Brás LE, Scherrer-Crosbie M. Guidelines for measuring cardiac physiology in mice. *Am J Physiol Heart Circ Physiol* 2018;**314**:H733-H752.
50. Liehn EA, Ponomariov V, Diaconu R, Streata I, Ioana M, Crespo-Avilan GE, Hernández-Reséndiz S, Cabrera-Fuentes HA. Apolipoprotein E in Cardiovascular Diseases: Novel Aspects of an Old-fashioned Enigma. *Arch Med Res* 2018;**49**:522-529.
51. Cox J, Mann M. 1D and 2D annotation enrichment: a statistical method integrating quantitative proteomics with complementary high-throughput data. *BMC Bioinformatics* 2012;**13 Suppl 16**:S12.
52. Gannon NP, Schnuck JK, Vaughan RA. BCAA Metabolism and Insulin Sensitivity - Dysregulated by Metabolic Status? *Mol Nutr Food Res* 2018;**62**:e1700756.
53. Foulquier S, Daskalopoulos EP, Lluri G, Hermans KCM, Deb A, Blankesteijn WM. WNT Signaling in Cardiac and Vascular Disease. *Pharmacol Rev* 2018;**70**:68-141.
54. Gordon JW, Shaw JA, Kirshenbaum LA. Multiple facets of NF-κB in the heart: to be or not to NF-κB. *Circ Res* 2011;**108**:1122-1132.
55. Yang S, Chen C, Wang H, Rao X, Wang F, Duan Q, Chen F, Long G, Gong W, Zou MH, Wang DW. Protective effects of Acyl-coA thioesterase 1 on diabetic heart via PPARα/PGC1α signaling. *PLoS One* 2012;**7**:e50376.
56. Pfeffer SR. NPC intracellular cholesterol transporter 1 (NPC1)-mediated cholesterol export from lysosomes. *J Biol Chem* 2019;**294**:1706-1709.
57. Chowaniec Z, Skoczyńska A. Plasma lipid transfer proteins: The role of PLTP and CETP in atherogenesis. *Adv Clin Exp Med* 2018;**27**:429-436.
58. Shi F, Sun L, Kaptoge S. Association of beta-2-microglobulin and cardiovascular events and mortality: A systematic review and meta-analysis. *Atherosclerosis* 2021;**320**:70-78.
59. Stragier B, De Bundel D, Sarre S, Smolders I, Vauquelin G, Dupont A, Michotte Y, Vanderheyden P. Involvement of insulin-regulated aminopeptidase in the effects of the renin-angiotensin fragment angiotensin IV: a review. *Heart Fail Rev* 2008;**13**:321-337.
60. Yang H, Zeng XJ, Wang HX, Zhang LK, Dong XL, Guo S, Du J, Li HH, Tang CS. Angiotensin IV protects against angiotensin II-induced cardiac injury via AT4 receptor. *Peptides* 2011;**32**:2108-2115.
61. Kosok M, Alli-Shaik A, Bay BH, Gunaratne J. Comprehensive Proteomic Characterization Reveals Subclass-Specific Molecular Aberrations within Triple-negative Breast Cancer. *iScience* 2020;**23**:100868.
62. Pillois X, Nurden AT. Linkage disequilibrium amongst ITGA2B and ITGB3 gene variants in patients with Glanzmann thrombasthenia confirms that most disease-causing mutations are recent. *Br J Haematol* 2016;**175**:686-695.
63. Khuchua Z, Glukhov AI, Strauss AW, Javadov S. Elucidating the Beneficial Role of PPAR Agonists in Cardiac Diseases. *Int J Mol Sci* 2018;**19**:3464.
64. Hornbeck PV, Kornhauser JM, Tkachev S, Zhang B, Skrzypek E, Murray B, Latham V, Sullivan M. PhosphoSitePlus: a comprehensive resource for investigating the structure and function of experimentally determined post-translational modifications in man and mouse. *Nucleic Acids Res* 2012;**40**:D261-270.

65. Kukreja RC, Salloum FN, Das A. Cyclic guanosine monophosphate signaling and phosphodiesterase-5 inhibitors in cardioprotection. *J Am Coll Cardiol* 2012;**59**:1921-1927.
66. de Lucia C, Wallner M, Eaton DM, Zhao H, Houser SR, Koch WJ. Echocardiographic Strain Analysis for the Early Detection of Left Ventricular Systolic/Diastolic Dysfunction and Dyssynchrony in a Mouse Model of Physiological Aging. *J Gerontol A Biol Sci Med Sci* 2019;**74**:455-461.
67. Mattson MP, Wan R. Beneficial effects of intermittent fasting and caloric restriction on the cardiovascular and cerebrovascular systems. *J Nutr Biochem* 2005;**16**:129-137.
68. Sutton EF, Beyl R, Early KS, Cefalu WT, Ravussin E, Peterson CM. Early Time-Restricted Feeding Improves Insulin Sensitivity, Blood Pressure, and Oxidative Stress Even without Weight Loss in Men with Prediabetes. *Cell Metab* 2018;**27**:1212-1221.e3.
69. Griffioen KJ, Rothman SM, Ladenheim B, Wan R, Vranis N, Hutchison E, Okun E, Cadet JL, Mattson MP. Dietary energy intake modifies brainstem autonomic dysfunction caused by mutant α-synuclein. *Neurobiol Aging* 2013;**34**:928-935.
70. Ma X, Mani K, Liu H, Kovacs A, Murphy JT, Foroughi L, French BA, Weinheimer CJ, Kraja A, Benjamin IJ, Hill JA, Javaheri A, Diwan A. Transcription Factor EB Activation Rescues Advanced αB-Crystallin Mutation-Induced Cardiomyopathy by Normalizing Desmin Localization. *J Am Heart Assoc* 2019;**8**:e010866.
71. Bruce-Keller AJ, Umberger G, McFall R, Mattson MP. Food restriction reduces brain damage and improves behavioral outcome following excitotoxic and metabolic insults. *Ann Neurol* 1999;**45**:8-15.
72. Johnson JB, Summer W, Cutler RG, Martin B, Hyun DH, Dixit VD, Pearson M, Nassar M, Telljohann R, Maudsley S, Carlson O, John S, Laub DR, Mattson MP. Alternate day calorie restriction improves clinical findings and reduces markers of oxidative stress and inflammation in overweight adults with moderate asthma. *Free Radic Biol Med* 2006;**42**:665-674.
73. Rengo G, Parisi V, Femminella GD, Pagano G, de Lucia C, Cannavo A, Liccardo D, Giallauria F, Scala O, Zincarelli C, Perrone Filardi P, Ferrara N, Leosco D. Molecular aspects of the cardioprotective effect of exercise in the elderly. *Aging Clin Exp Res* 2013;**25**:487-497.
74. Voulgari C, Pagoni S, Vinik A, Poirier P. Exercise improves cardiac autonomic function in obesity and diabetes. *Metabolism* 2013;**62**:609-621.
75. Drake JC, Wilson RJ, Yan Z. Molecular mechanisms for mitochondrial adaptation to exercise training in skeletal muscle. *FASEB J* 2016;**30**:13-22.
76. Bernardo BC, Ooi JYY, Weeks KL, Patterson NL, McMullen JR. Understanding Key Mechanisms of Exercise-Induced Cardiac Protection to Mitigate Disease: Current Knowledge and Emerging Concepts. *Physiol Rev* 2018;**98**:419-475.
77. Liu D, Zhang Y, Gharavi R, Park HR, Lee J, Siddiqui S, Telljohann R, Nassar MR, Cutler RG, Becker KG, Mattson MP. The mitochondrial uncoupler DNP triggers brain cell mTOR signaling network reprogramming and CREB pathway up-regulation. *J Neurochem* 2015;**134**:677-692.
78. Wan R, Camandola S, Mattson MP. Dietary supplementation with 2-deoxy-D-glucose improves cardiovascular and neuroendocrine stress adaptation in rats. *Am J Physiol Heart Circ Physiol* 2004;**287**:H1186-193.
79. Yu ZF, Mattson MP. Dietary restriction and 2-deoxyglucose administration reduce focal ischemic brain damage and improve behavioral outcome: evidence for a preconditioning mechanism. *J Neurosci Res* 1999;**57**:830-839.
80. Cox PJ, Kirk T, Ashmore T, Willerton K, Evans R, Smith A, Murray AJ, Stubbs B, West J, McLure SW, King MT, Dodd MS, Holloway C, Neubauer S, Drawer S, Veech RL,

Griffin JL, Clarke K. Nutritional Ketosis Alters Fuel Preference and Thereby Endurance Performance in Athletes. *Cell Metab* 2016;**24**:256-268.
81. Kashiwaya Y, Bergman C, Lee JH, Wan R, King MT, Mughal MR, Okun E, Clarke K, Mattson MP, Veech RL. A ketone ester diet exhibits anxiolytic and cognition-sparing properties, and lessens amyloid and tau pathologies in a mouse model of Alzheimer's disease. *Neurobiol Aging* 2013;**34**:1530-1539.
82. Sciarretta S, Volpe M, Sadoshima J. Mammalian target of rapamycin signaling in cardiac physiology and disease. *Circ Res* 2014;**114**:549-564.
83. Franklin MP, Sathyanarayan A, Mashek DG. Acyl-CoA Thioesterase 1 (ACOT1) Regulates PPARα to Couple Fatty Acid Flux With Oxidative Capacity During Fasting. *Diabetes* 2017;**66**:2112-2123.
84. Lazennec G, Canaple L, Saugy D, Wahli W. Activation of peroxisome proliferator-activated receptors (PPARs) by their ligands and protein kinase A activators. *Mol Endocrinol* 2000;**14**:1962-1975.
85. Brushia RJ, Walsh DA. Phosphorylase kinase: the complexity of its regulation is reflected in the complexity of its structure. *Front Biosci*. 1999;**4**:D618-641.
86. Bockus LB, Humphries KM. cAMP-dependent Protein Kinase (PKA) Signaling Is Impaired in the Diabetic Heart. *J Biol Chem* 2015;**290**:29250-29258.
87. Callaghan NI. β-Adrenergic augmentation of cardiac contractility is dependent on PKA-mediated phosphorylation of myosin-binding protein C and troponin I. *J Physiol* 2016;**594**:4707-4708.
88. Lissandron V, Zaccolo M. Compartmentalized cAMP/PKA signalling regulates cardiac excitation-contraction coupling. *J Muscle Res Cell Motil* 2006;**27**:399-403.
89. Jessen N, An D, Lihn AS, Nygren J, Hirshman MF, Thorell A, Goodyear LJ. Exercise increases TBC1D1 phosphorylation in human skeletal muscle. *Am J Physiol Endocrinol Metab* 2011;**301**:E164-171.
90. Mueckler M. Insulin resistance and the disruption of Glut4 trafficking in skeletal muscle. *J Clin Invest* 2001;**107**:1211-1213.
91. LeWinter MM, Granzier HL. Cardiac titin and heart disease. J Cardiovasc Pharmacol 2014;63:207-212.
92. Makarenko I, Opitz CA, Leake MC, Neagoe C, Kulke M, Gwathmey JK, del Monte F, Hajjar RJ, Linke WA. Passive stiffness changes caused by upregulation of compliant titin isoforms in human dilated cardiomyopathy hearts. Circ Res 2004;95:708-716.
93. Zhou P, Pu WT. Recounting Cardiac Cellular Composition. *Circ Res* 2016;**118**:368-370.
94. Damiola F, Le Minh N, Preitner N, Kornmann B, Fleury-Olela F, Schibler U. Restricted feeding uncouples circadian oscillators in peripheral tissues from the central pacemaker in the suprachiasmatic nucleus. *Genes Dev* 2000;**14**:2950-2961.
95. Hara R, Wan K, Wakamatsu H, Aida R, Moriya T, Akiyama M, Shibata S. Restricted feeding entrains liver clock without participation of the suprachiasmatic nucleus. *Genes Cells* 2001;**6**:269-278.
96. Stokkan KA, Yamazaki S, Tei H, Sakaki Y, Menaker M. Entrainment of the circadian clock in the liver by feeding. Science 2001;**291**:490-493.

Figure legends

Figure 1. Impact of intermittent fasting on the heart proteome

(a) Hierarchical clustering of proteins significantly differentially expressed in each IF group and AL group (one-way ANOVA with Dunnett's test). The color scale denotes z-score normalized protein abundances. Red denotes higher protein abundance, and blue lower protein abundance. Gene ontology-based biological processes and pathways significantly enriched in representative protein clusters across the different groups. Selected enzymes specifically modulated within each cluster are highlighted. **(b)** IF-modulated kinases involved in metabolic pathways and signaling pathways. **(c)** Enrichment analysis of modulated processes and pathways in the different IF groups in comparison to the AL group (1-D annotation enrichment using Wilcoxon-Mann-Whitney test). Each dot represents a functional process or pathway. A positive enrichment score denotes higher protein abundance, and a negative enrichment score denotes lower protein abundance. n = 4-5 mice in each experimental group.

Figure 2. Differential effects of IF regimen functional processes

(a) Functional transition network that shows functional remodeling of heart proteome in response to IF12 (a), IF16 (b), and EOD (c) GSEA for biological processes and pathways performed for each IF regimen comparison is shown as an enrichment map. Functions significantly enriched ($p < 0.01$, nominal p-value from empirical phenotype-based permutation test in GSEA) among the upregulated and downregulated proteins for each comparison are indicated by red and blue nodes, respectively. The size of the nodes indicates the number of proteins within the node and edges link nodes that share common proteins. **(d)** Functional processes and pathways altered by changes in transcriptome and proteome abundances through different IF regimens (Benjamini-Hochberg FDR < 0.05, 2-D annotation enrichment using MANOVA test). Each dot on the plot represents a modulation in pathway or process. The scores indicate abundance changes of transcriptome or proteome levels over AL. Upregulation and downregulation of components are denoted by positive and negative scores, respectively. n = 4-5 mice in each experimental group.

Figure 3. Network mapping of IF-responsive proteins

(a) Proteins with significantly altered abundance in response to IF that are overlaid on consensus protein-protein interaction network constructed using all IF-responsive proteins. The proteins that sequentially show differential modulation are indicated with different colors as yellow (IF12), blue (IF16), and red (EOD). **(b)** The top densely connected functional protein clusters are shown (one-sided Mann-Whitney U test as implemented in Cluster ONE). The color of each node indicates the IF regimen for which the protein was differentially expressed. Yellow, blue and red indicate IF12, IF16 and EOD regimens, respectively. The heat maps show proteome changes for the proteins in the respective clusters. Red denotes increased expression, and blue denotes decreased expression. **(c)** Transcription factors significantly enriched across the different IF groups. n = 4-5 mice in each experimental group.

Figure 4. Phosphoproteome landscape of IF-induced changes in heart

(a) Phosphorylation sites showing significant changes in the hearts of mice in the IF12, IF16, and EOD. Phosphorylation changes observed on structural sarcomere organization proteins are highlighted. **(b)** Hierarchical clustering of differentially altered phosphopeptides showing increased (red) and decreased (blue) phosphosite abundance. Kinase motifs enriched ($p < 0.05$) in representative clusters are shown (Fisher's exact test for enrichment). **(c)** Pathways significantly enriched (p-value ≤ 0.05) among the differentially altered phosphoproteins across the three IF regimens are visualized as a heatmap (Fisher's exact test for enrichment). The color scale represents negative log10-transformed p values. **(d)** Temporal alteration of specific IF-responsive phosphorylation sites in AMPK and cGMP-PKG signaling. n = 3 mice in each experimental group.

Figure 5. Immunoblot validation of the selected proteins in IF-modulated pathways

(a) Immunoblots that show the effects of IF16 on the expression of selected proteins p-AMPKα/AMPKα, PKG-1, MYPT1, PPARγ, p-GSKαβ/GSKαβ, AKT, p-IRS1/IRS-1 and Insulin receptor β compared to AL group. Data are represented as mean ± S.E.M. n = 6 mice in each experimental group. *$p < 0.05$ compared with young Sham; **$p < 0.01$ compared with AL group.

Figure 6. Echocardiographic analyses of IF on cardiac stress adaptation

(a) Dobutamine stress tests for ability of the heart to adapt to stress under IF. Heart rate and ejection fraction following administration of dobutamine were measured. Values are the mean ± SD; n=10 each; *$p < 0.05$ (Unpaired t-test). Representative images of long axis M-Mode

raw data before and after dobutamine-induced stress are shown in the right panel. **(b)** Contractility in hearts of IF16 mice compared with AL mice as illustrated by global longitudinal strain (GLS) (upper panel) and radial strain (lower panel). Values are the mean ± SD (n = 10 in each experimental group; **$p < 0.01$, ***$p < 0.001$) before and after dobutamine (one-way ANOVA with Tukey's multiple comparisons test). Representative images of myocardial movement (upper panel) and radial strain (lower panel) before and after dobutamine-induced stress.

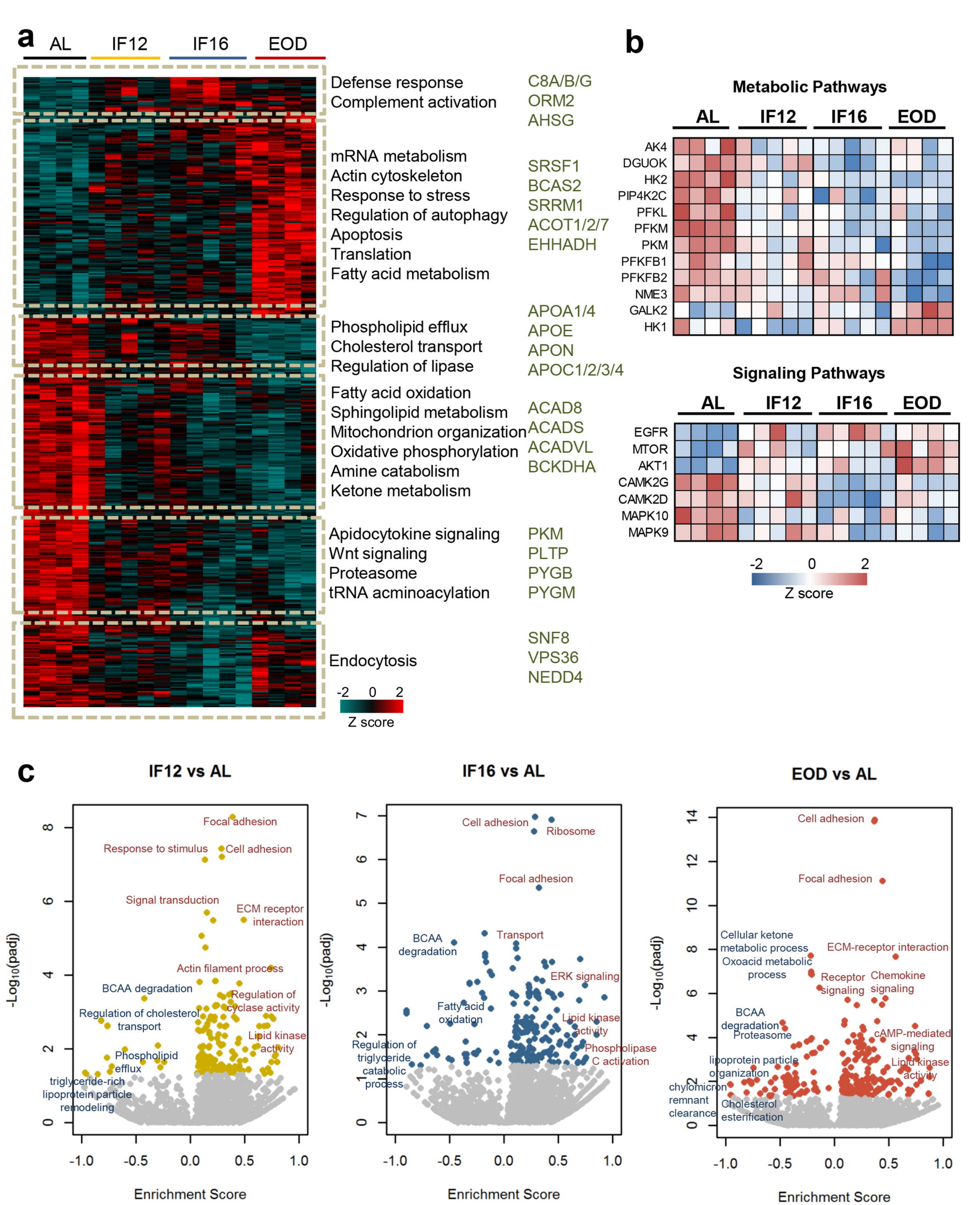
a
AL
IF12
IF16
EOD
Defense response
Complement activation
mRNA metabolism
Actin cytoskeleton
Response to stress
Regulation of autophagy
Apoptosis
Translation
Fatty acid metabolism
Phospholipid efflux
Cholesterol transport
Regulation of lipase
Fatty acid oxidation
Sphingolipid metabolism
Mitochondrion organization
Oxidative phosphorylation
Amine catabolism
Ketone metabolism
Apidocytokine signaling
Wnt signaling
Proteasome
tRNA acminoacylation
Endocytosis
C8A/B/G
ORM2
AHSG
SRSF1
BCAS2
SRRM1
ACOT1/2/7
EHHADH
APOA1/4
APOE
APON
APOC1/2/3/4
ACAD8
ACADS
ACADVL
BCKDHA
PKM
PLTP
PYGB
PYGM
SNF8
VPS36
NEDD4
-2 0 2
Z score
b
Metabolic Pathways
AL IF12 IF16 EOD
AK4
DGUOK
HK2
PIP4K2C
PFKL
PFKM
PKM
PFKFB1
PFKFB2
NME3
GALK2
HK1
Signaling Pathways
AL IF12 IF16 EOD
EGFR
MTOR
AKT1
CAMK2G
CAMK2D
MAPK10
MAPK9
-2 0 2
Z score
c
IF12 vs AL
Focal adhesion
Response to stimulus
Cell adhesion
Signal transduction
ECM receptor interaction
Actin filament process
BCAA degradation
Regulation of cyclase activity
Regulation of cholesterol transport
Lipid kinase activity
Phospholipid efflux
triglyceride-rich lipoprotein particle remodeling
-Log10(padj)
Enrichment Score
IF16 vs AL
Cell adhesion
Ribosome
Focal adhesion
Transport
BCAA degradation
ERK signaling
Fatty acid oxidation
Lipid kinase activity
Regulation of triglyceride catabolic process
Phospholipase C activation
-Log10(padj)
Enrichment Score
EOD vs AL
Cell adhesion
Focal adhesion
Cellular ketone metabolic process
ECM-receptor interaction
Oxoacid metabolic process
Receptor signaling
Chemokine signaling
BCAA degradation
Proteasome
cAMP-mediated signaling
lipoprotein particle organization
Lipid kinase activity
chylomicron remnant clearance
Cholesterol esterification
-Log10(padj)
Enrichment Score

Figure 1

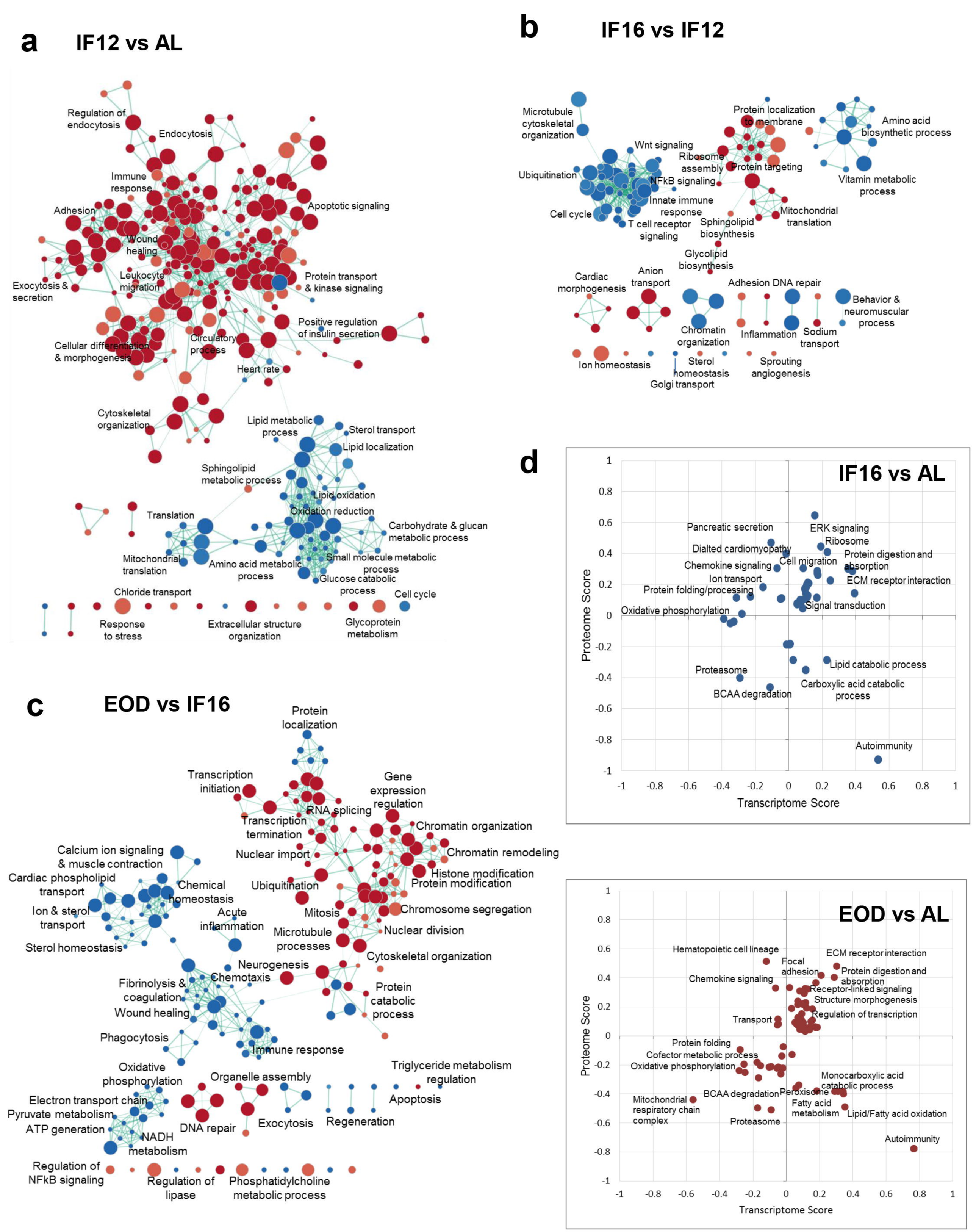
a
IF12 vs AL
Regulation of endocytosis
Endocytosis
Immune response
Adhesion
Apoptotic signaling
Wound healing
Leukocyte migration
Exocytosis & secretion
Protein transport & kinase signaling
Positive regulation of insulin secretion
Cellular differentiation & morphogenesis
Circulatory process
Heart rate
Cytoskeletal organization
Lipid metabolic process
Sterol transport
Lipid localization
Sphingolipid metabolic process
Lipid oxidation
Translation
Oxidation reduction
Carbohydrate & glucan metabolic process
Mitochondrial translation
Amino acid metabolic process
Small molecule metabolic process
Glucose catabolic process
Chloride transport
Cell cycle
Response to stress
Extracellular structure organization
Glycoprotein metabolism
b
IF16 vs IF12
Microtubule cytoskeletal organization
Protein localization to membrane
Amino acid biosynthetic process
Wnt signaling
Ribosome assembly
Protein targeting
Ubiquitination
NFkB signaling
Vitamin metabolic process
Innate immune response
Cell cycle
Mitochondrial translation
T cell receptor signaling
Sphingolipid biosynthesis
Glycolipid biosynthesis
Cardiac morphogenesis
Anion transport
Adhesion DNA repair
Behavior & neuromuscular process
Chromatin organization
Inflammation
Sodium transport
Ion homeostasis
Sterol homeostasis
Sprouting angiogenesis
Golgi transport
c
EOD vs IF16
Protein localization
Transcription initiation
Gene expression regulation
RNA splicing
Transcription termination
Chromatin organization
Calcium ion signaling & muscle contraction
Nuclear import
Chromatin remodeling
Cardiac phospholipid transport
Histone modification
Protein modification
Chemical homeostasis
Ubiquitination
Ion & sterol transport
Acute inflammation
Mitosis
Chromosome segregation
Sterol homeostasis
Microtubule processes
Nuclear division
Cytoskeletal organization
Neurogenesis
Chemotaxis
Fibrinolysis & coagulation
Protein catabolic process
Wound healing
Phagocytosis
Immune response
Oxidative phosphorylation
Triglyceride metabolism regulation
Organelle assembly
Electron transport chain
Apoptosis
Pyruvate metabolism
ATP generation
DNA repair
Exocytosis
Regeneration
NADH metabolism
Regulation of NFkB signaling
Regulation of lipase
Phosphatidylcholine metabolic process
d
IF16 vs AL
Proteome Score
Transcriptome Score
Pancreatic secretion
ERK signaling
Ribosome
Dialted cardiomyopathy
Protein digestion and absorption
Chemokine signaling
Cell migration
Ion transport
ECM receptor interaction
Protein folding/processing
Signal transduction
Oxidative phosphorylation
Lipid catabolic process
Proteasome
Carboxylic acid catabolic process
BCAA degradation
Autoimmunity
EOD vs AL
Hematopoietic cell lineage
ECM receptor interaction
Focal adhesion
Protein digestion and absorption
Chemokine signaling
Receptor-linked signaling
Structure morphogenesis
Transport
Regulation of transcription
Protein folding
Cofactor metabolic process
Oxidative phosphorylation
Monocarboxylic acid catabolic process
BCAA degradation
Peroxisome
Mitochondrial respiratory chain complex
Fatty acid metabolism
Lipid/Fatty acid oxidation
Proteasome
Autoimmunity

Figure 2

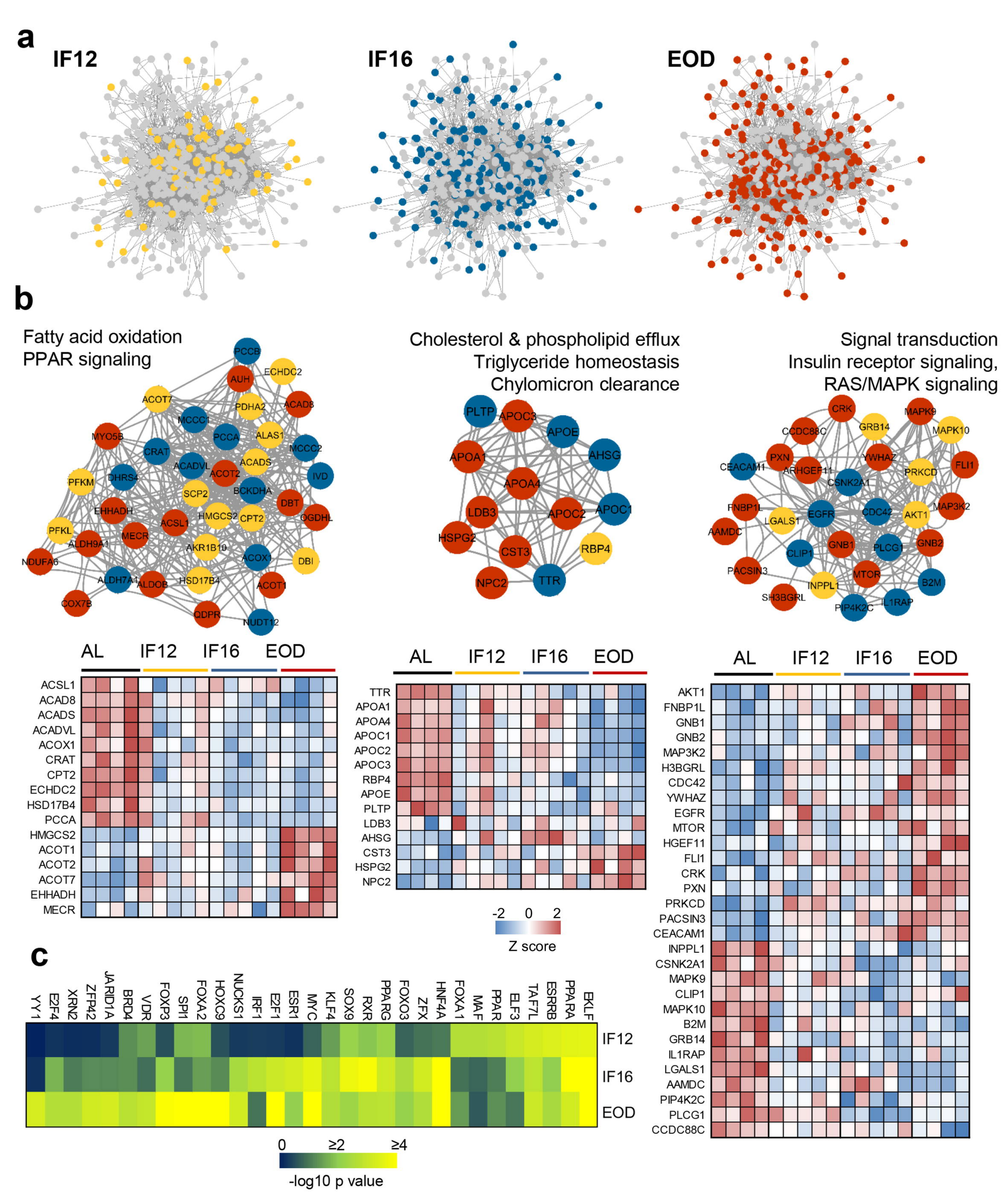
a
IF12
IF16
EOD
b
Fatty acid oxidation
PPAR signaling
PCCB
ECHDC2
AUH
ACOT7
PDHA2
ACAD8
MCCC1
MYO5B
PCCA
ALAS1
CRAT
MCCC2
ACADVL
ACADS
ACOT2
IVD
PFKM
DHRS4
SCP2
BCKDHA
DBT
EHHADH
HMGCS2
CPT2
OGDHL
ACSL1
PFKL
MECR
ALDH9A1
AKR1B10
NDUFA6
ACOX1
DBI
ALDH7A1
ALDOB
HSD17B4
ACOT1
COX7B
QDPR
NUDT12
Cholesterol & phospholipid efflux
Triglyceride homeostasis
Chylomicron clearance
PLTP
APOC3
APOE
APOA1
AHSG
APOA4
LDB3
APOC2
APOC1
HSPG2
CST3
RBP4
NPC2
TTR
Signal transduction
Insulin receptor signaling,
RAS/MAPK signaling
CRK
MAPK9
CCDC88C
GRB14
MAPK10
PXN
YWHAZ
CEACAM1
ARHGEF11
PRKCD
FLI1
CSNK2A1
FNBP1L
EGFR
CDC42
AKT1
MAP3K2
LGALS1
AAMDC
GNB1
PLCG1
GNB2
CLIP1
PACSIN3
MTOR
B2M
INPPL1
SH3BGRL
PIP4K2C
IL1RAP
AL
IF12
IF16
EOD
ACSL1
ACAD8
ACADS
ACADVL
ACOX1
CRAT
CPT2
ECHDC2
HSD17B4
PCCA
HMGCS2
ACOT1
ACOT2
ACOT7
EHHADH
MECR
TTR
APOA1
APOA4
APOC1
APOC2
APOC3
RBP4
APOE
PLTP
LDB3
AHSG
CST3
HSPG2
NPC2
-2
0
2
Z score
AKT1
FNBP1L
GNB1
GNB2
MAP3K2
H3BGRL
CDC42
YWHAZ
EGFR
MTOR
HGEF11
FLI1
CRK
PXN
PRKCD
PACSIN3
CEACAM1
INPPL1
CSNK2A1
MAPK9
CLIP1
MAPK10
B2M
GRB14
IL1RAP
LGALS1
AAMDC
PIP4K2C
PLCG1
CCDC88C
c
YY1
E2F4
XRN2
ZFP42
JARID1A
BRD4
VDR
FOXP3
SPI1
FOXA2
HOXC9
NUCKS1
IRF1
E2F1
ESR1
MYC
KLF4
SOX9
RXR
PPARG
FOXO3
ZFX
HNF4A
FOXA1
MAF
PPAR
ELF3
TAF7L
ESRRB
PPARA
EKLF
IF12
IF16
EOD
0
≥2
≥4
-log10 p value

Figure 3

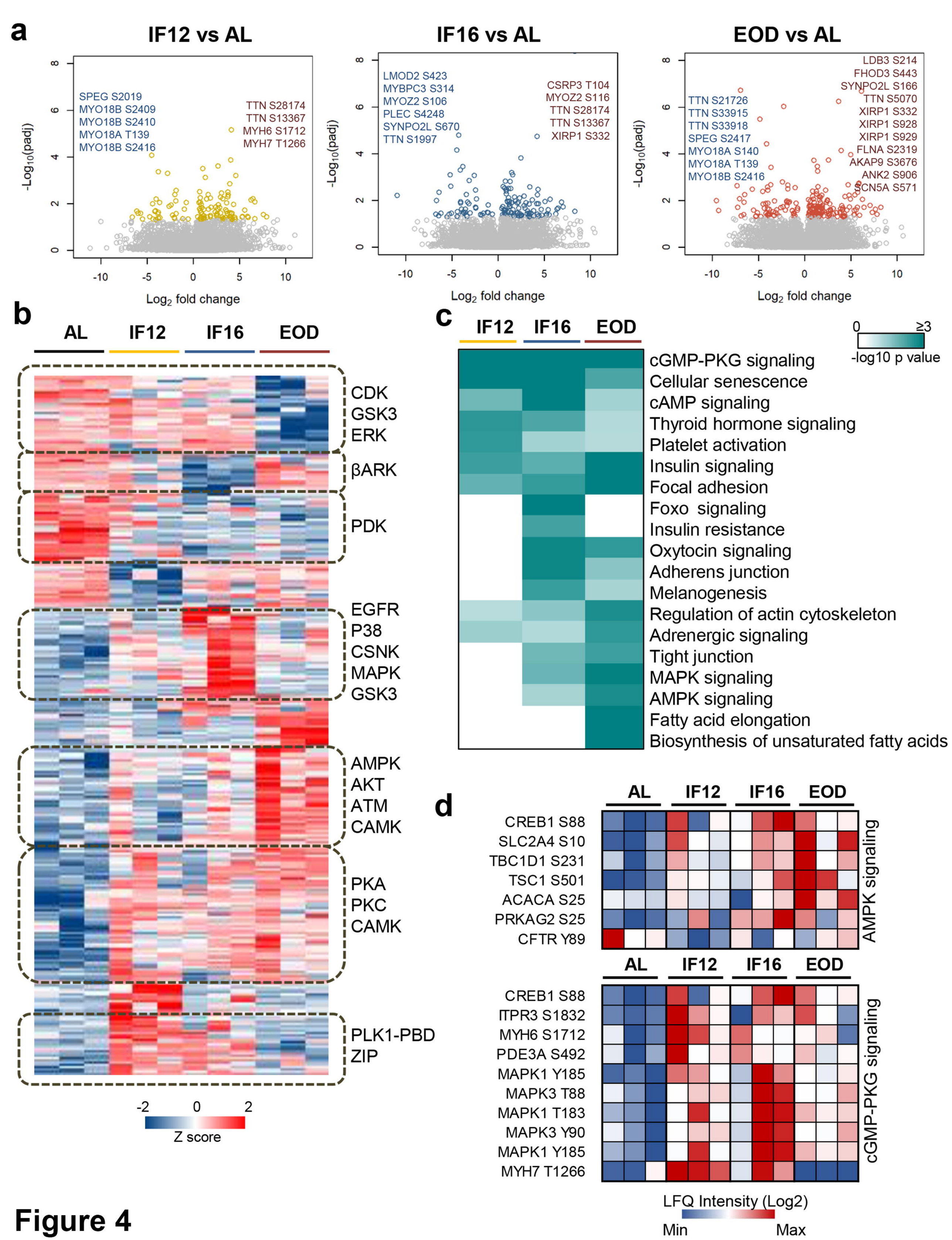
a
IF12 vs AL
IF16 vs AL
EOD vs AL
-Log10(padj)
Log2 fold change
SPEG S2019
MYO18B S2409
MYO18B S2410
MYO18A T139
MYO18B S2416
TTN S28174
TTN S13367
MYH6 S1712
MYH7 T1266
LMOD2 S423
MYBPC3 S314
MYOZ2 S106
PLEC S4248
SYNPO2L S670
TTN S1997
CSRP3 T104
MYOZ2 S116
TTN S28174
TTN S13367
XIRP1 S332
TTN S21726
TTN S33915
TTN S33918
SPEG S2417
MYO18A S140
MYO18A T139
MYO18B S2416
LDB3 S214
FHOD3 S443
SYNPO2L S166
TTN S5070
XIRP1 S332
XIRP1 S928
XIRP1 S929
FLNA S2319
AKAP9 S3676
ANK2 S906
SCN5A S571
b
AL
IF12
IF16
EOD
CDK
GSK3
ERK
βARK
PDK
EGFR
P38
CSNK
MAPK
GSK3
AMPK
AKT
ATM
CAMK
PKA
PKC
CAMK
PLK1-PBD
ZIP
Z score
c
IF12
IF16
EOD
-log10 p value
cGMP-PKG signaling
Cellular senescence
cAMP signaling
Thyroid hormone signaling
Platelet activation
Insulin signaling
Focal adhesion
Foxo signaling
Insulin resistance
Oxytocin signaling
Adherens junction
Melanogenesis
Regulation of actin cytoskeleton
Adrenergic signaling
Tight junction
MAPK signaling
AMPK signaling
Fatty acid elongation
Biosynthesis of unsaturated fatty acids
d
CREB1 S88
SLC2A4 S10
TBC1D1 S231
TSC1 S501
ACACA S25
PRKAG2 S25
CFTR Y89
AMPK signaling
CREB1 S88
ITPR3 S1832
MYH6 S1712
PDE3A S492
MAPK1 Y185
MAPK3 T88
MAPK1 T183
MAPK3 Y90
MAPK1 Y185
MYH7 T1266
cGMP-PKG signaling
LFQ Intensity (Log2)
Min
Max

Figure 4

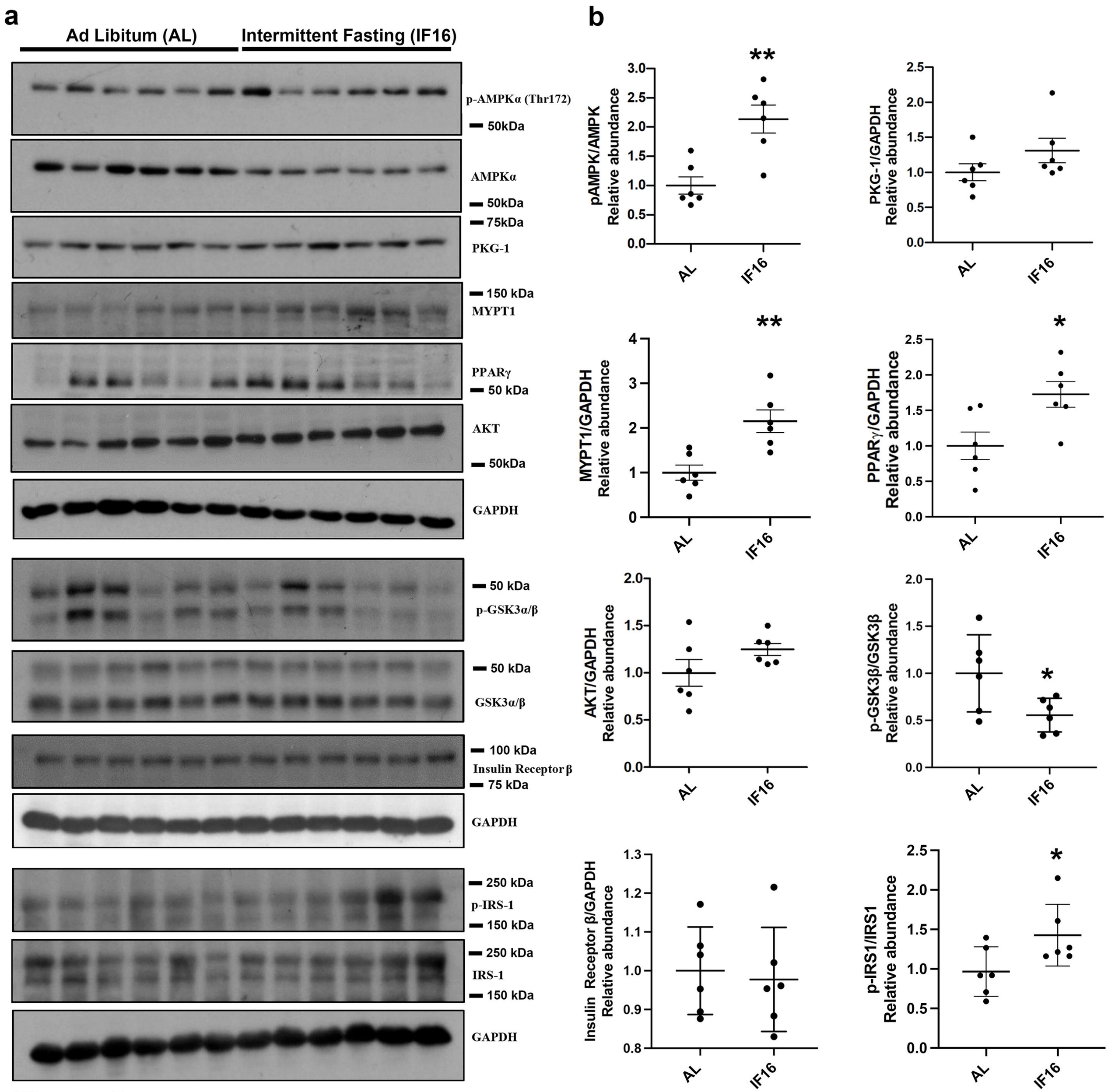
a
Ad Libitum (AL)
Intermittent Fasting (IF16)
p-AMPKα (Thr172)
50kDa
AMPKα
50kDa
75kDa
PKG-1
150 kDa
MYPT1
PPARγ
50 kDa
AKT
50kDa
GAPDH
50 kDa
p-GSK3α/β
50 kDa
GSK3α/β
100 kDa
Insulin Receptor β
75 kDa
GAPDH
250 kDa
p-IRS-1
150 kDa
250 kDa
IRS-1
150 kDa
GAPDH
b
pAMPK/AMPK Relative abundance
PKG-1/GAPDH Relative abundance
MYPT1/GAPDH Relative abundance
PPARγ/GAPDH Relative abundance
AKT/GAPDH Relative abundance
p-GSK3β/GSK3β Relative abundance
Insulin Receptor β/GAPDH Relative abundance
p-IRS1/IRS1 Relative abundance
AL
IF16

Figure 5

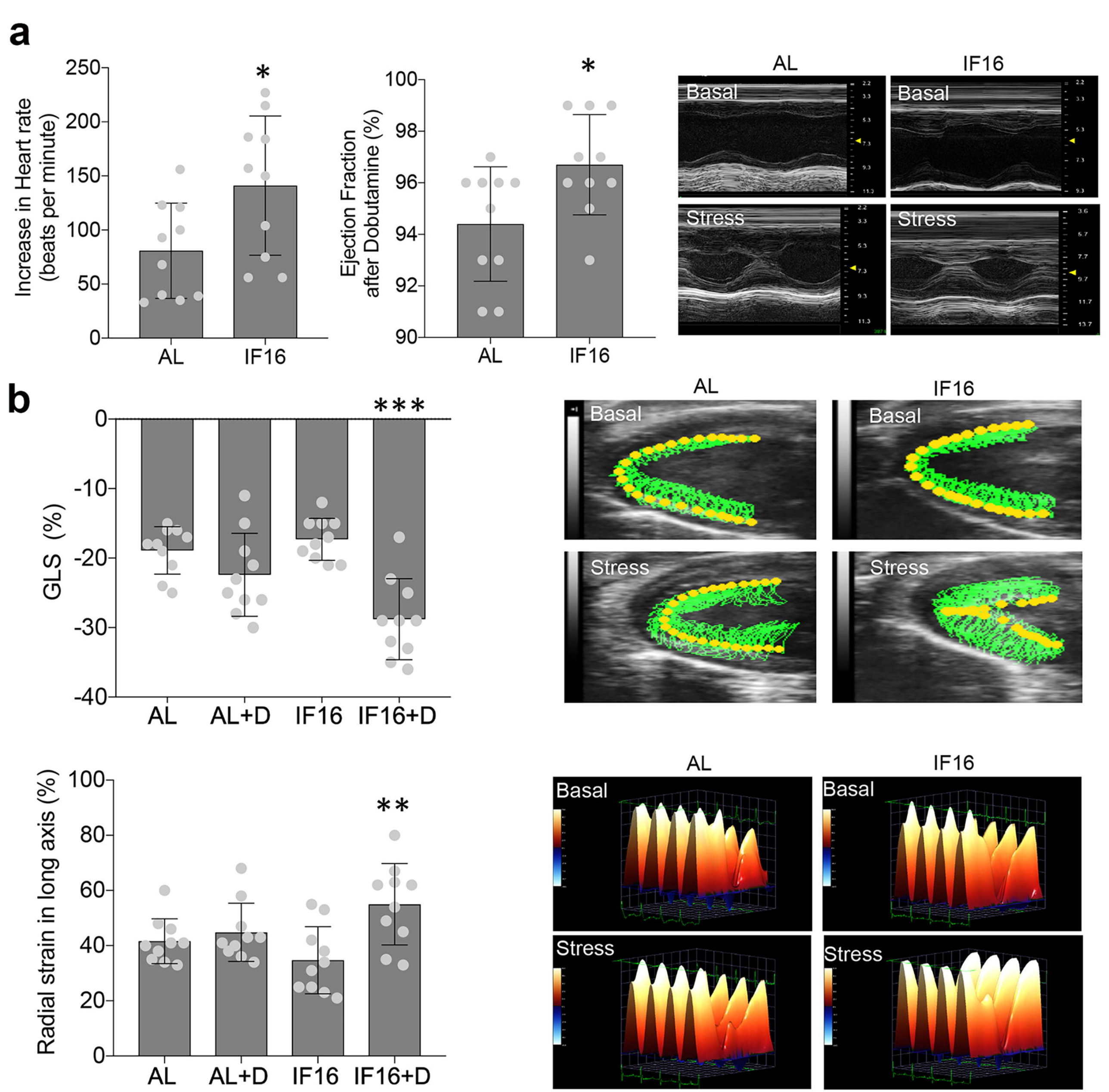
a
Increase in Heart rate (beats per minute)
250
200
150
100
50
0
*
AL
IF16
Ejection Fraction after Dobutamine (%)
100
98
96
94
92
90
*
AL
IF16
AL
IF16
Basal
Basal
Stress
Stress
b
GLS (%)
0
-10
-20
-30
-40
***
AL
AL+D
IF16
IF16+D
AL
IF16
Basal
Basal
Stress
Stress
Radial strain in long axis (%)
100
80
60
40
20
0
**
AL
AL+D
IF16
IF16+D
AL
IF16
Basal
Basal
Stress
Stress

Figure 6